Model development and validation of an industrial natural gas well production network

by

Rudzani Dzedzemane

Submitted in partial fulfillment of the requirements for the degree

Master of Engineering (Electronic Engineering)

in the

Department of Electrical, Electronic and Computer Engineering

Faculty of Engineering, Built Environment and Information Technology

UNIVERSITY OF PRETORIA

October 2024

SUMMARY

Model development and validation of an industrial natural gas well production network

by

Rudzani Dzedzemane

Supervisor:	Prof Ian K. Craig
Co-supervisor:	Prof J. Derik le Roux
Department:	Electrical, Electronic and Computer Engineering
University:	University of Pretoria
Degree:	Master of Engineering (Electronic Engineering)
Keywords:	Characteristic compatibility method, gas pipelines, natural gas well, parameter estimation, spectral element method, dynamic model validation

A transient state-space non-linear model is developed for a natural gas production network fed from multiple gas wellheads. The state-space model is developed by making use of the spectral element method for pipeline spatial discretization. Wellhead models are integrated into the pipeline models by making use of suitable boundary conditions based on the characteristic compatibility method. The models are validated against a large scale natural gas well production network. The validation shows that the model has a good prediction performance based on a low normalized root mean square error of at most 5.08% and a high Pearson correlation coefficient with measured plant data of at least 0.94. The good prediction response of the developed transient models make them suitable for use in model-based optimal control of natural gas well production networks. The resulting dynamic model can be easily adapted to a gas network of any configuration due to its modular form.

LIST OF ABBREVIATIONS

CCM	Characteristic compatibility method
CV	Controlled variable
DV	Disturbance variable
FEM	Finite element method
FVM	Finite volume method
LGL	Legendre-Gauss-Lobatto
MPC	Model predictive control
MOC	Method of characteristics
MV	Manipulated variable
PFD	Process flow diagram
RMSE	Root mean square error
SEM	Spectral element method

TABLE OF CONTENTS

LIST OF FIGURES

LIST OF TABLES

CHAPTER 1 INTRODUCTION

1.1 PROBLEM STATEMENT AND BACKGROUND

Natural gas is an energy source that has a higher efficiency as compared to coal and oil. It also releases less harmful products when burnt (Wang and Economides, 2009). Therefore, it has the potential to play an important role in the decarbonisation of a coal based economies such as South Africa, Poland, India and China where 90% (Strambo et al., 2019), 72% (*International Energy Agency*, n.d.), 71% (*International Energy Agency*, n.d.) and 60% (Tordoir, 2022) of electricity is generated from coal respectively. The importance of using natural gas as an intermediary energy source has been recognized by the industrial sector which aims to use natural gas in its transition to net-zero emissions (*Climate Change Report for the year ended 30 June 2021*, 2021; *The role of gas as a transition fuel in South Africa's path to net-zero*, 2022). The highlighted importance of natural gas in energy decarbonization justifies research into the optimal control of upstream natural gas production systems.

A natural gas well production system is typically a multiple-input multiple-output (MIMO) system with multiple natural gas wells feeding a header that supplies multiple consumers. The production network is highly interactive as a change in gas flow from one well can affect the flow of gas from all other wells in the network. A natural gas production network has constraints on the gas flow rates from each well. A flow rate that is too high can result in water coning and deliver an undesired amount of water to the processing facility (Guo and Ghalambor, 2012). A low flow rate can result in liquid loading which occurs when the gas velocity is too low to carry condensate or liquids with the gas stream. The liquid can accumulate in the wellbore. If the accumulation problem is not rectified, production from the well may stop and the well will be abandoned (Bopbekov et al., 2022). The constraint on the gas flows from the wells further makes this a constrained MIMO system.

Constrained MIMO systems can be effectively controlled by making use of model predictive control

(MPC) (Darby and Nikolaou, 2012). Implementation of model predictive control however requires a dynamic model of the process, therefore this research investigates the development and validation of such a model for a natural gas well production network. The developed model shall be in a form that is suitable for use in model predictive control applications.

The following research gaps were identified:

- A transient model for a natural gas production network that includes the effects of gas well operation has not been researched

1.2 RESEARCH OBJECTIVE AND QUESTIONS

The main objective of this study is to develop a transient model of a gas production network that can be applied to model based control applications. Due to the nonlinear nature of gas networks, the model is developed using a first principles approach that includes first principle models of common gas production network components. These components are gas pipelines, choke valves and natural gas wells. Parameters that cannot be calculated or measured in the first principles model will be estimated from collected plant data. In developing the gas production network transient model the following research questions are considered:

- How can an accurate transient model for a gas production network be developed using a first principles approach?
- How can the gas wellhead production model be incorporated into the first principles production network model?
- How can the gas wellhead choke valve model be incorporated into the first principles production network model?

1.3 APPROACH

The research questions where answered using the following steps:

- Identify an industrial gas production network for use in validating the developed model
- Develop a first principles state-space transient model for the identified industrial gas production network
- Collect running plant data from the identified gas production network and use the collected plant data to validate the accuracy of the developed model

1.4 RESEARCH CONTRIBUTION

This dissertation extends on the work in Wiid et al. (2020) to include a model of the natural gas wells feeding the pipeline. The dynamic model is validated against online industrial plant data (Wiid et al., 2020; Burchell et al., 2023; Muller et al., 2011; Trapp et al., 2014; Walters et al., 2016; van de Haar et al., 2017).

The novelty in this dissertation is the implementation of the Spectral Element Method (SEM) to a large number of interconnected pipelines and the subsequent development of suitable boundary conditions for the gas wells, choke valves, and consumers with the aim of obtaining an overall numerically stable gas network model.

1.5 RESEARCH OUTPUTS

The following publications resulted from this study:

- Dzedzemane, R., le Roux, J. D., Muller, C. J. and Craig, I. (2018). Steam header state-space model development and validation, In 5th IFAC Workshop on Mining, Mineral and Metal Processing MMM 2018, Shanghai, China, 23–25 August, Vol. 51, pp. 207–212.
- Dzedzemane, R., Wiid, A. J., le Roux, J. D. and Craig, I. K. (2024). Natural gas well production network state-space model development and validation for process control, *Industrial & Engineering Chemistry Research* **63**(3): 1461–1473

1.6 OVERVIEW OF STUDY

The thesis is organized as follows:

- Chapter 2 describes the dynamic model of the individual components of a gas production network. These components are the gas pipelines, gas wellheads, and flow regulating choke valves.
- The gas production network individual component models developed in Chapter 2 are combined using suitable boundary conditions in Chapter 3 in order to develop an overall system model
- Chapter 4 presents the method used to determine unknown parameters in the developed gas production network model. The parameter estimation results are also presented in this chapter. The chapter also presents the results obtained from validating the developed model against collected plant data

- Chapter 5 concludes the dissertation and provides recommendations for future work based on the study outcomes

CHAPTER 2 MODELLING INDIVIDUAL ELEMENTS OF A NATURAL GAS NETWORK

2.1 CHAPTER OVERVIEW

This chapter presents the development of a state-space model for a single gas pipeline and, steady-state models for components of a natural gas production network. Section 2.2 presents a review of literature available on dynamic modelling of gas pipelines. Section 2.3 presents the physical laws and equations used in deriving the gas pipeline state-space models. In Section 2.4 the SEM is used to discretize the continuous space pipeline model into a discrete space form while Section 2.5 presents the method used to discretize the continuos time pipeline models. The boundary conditions required to finalize the solution of the gas pipeline hyperbolic differential equation model are defined in section 2.6. The mathematical equations used to calculate the values of unknown model parameters such as gas compressibility factor and pipe friction factor are presented in Section 2.7. Section 2.8 presents the steady-state model that defines the productivity of the natural gas well and Section 2.9 defines the steady-state models of the gas well choke valves.

2.2 LITERATURE REVIEW

The natural gas production network under consideration is made up of natural gas wells, choke valves for flow regulation, and networks of gas pipelines. This chapter presents the mathematical models of these natural gas production network components. The model development described in this chapter has already been published in Dzedzemane et al. (2024).

The first natural gas component to be considered is the natural gas pipeline networks. These pipelines transport the gas from the natural gas wellheads to a central processing facility. Considerable work has already been done on developing transient models of gas pipeline networks. The transient models are composed of hyperbolic partial differential equations which increases the complexity of the model

development problem. The hyperbolic partial differential equations can be solved for the network pressure and flow transients by making use of finite difference methods (FDM), (Koo, 2022) finite volumn methods (FVM),(Bermúdez and Shabani, 2019; Zienkiewicz and Taylor, 2000) finite element methods (FEM), (Koo, 2022; Twyman, 2018) the method of characteristics (MOC), (Canuto et al., 2007; Mennemann et al., 2018; Wiid et al., 2020) and spectral element methods (SEM).

Su et al. (2022) developed a linearized transient model of a pipeline network by making use of the FDM for spacial discretization. The resulting model accuracy was evaluated by comparing its performance against previous models and simulation software. The linearization, however, can result in model errors that can negatively affect the performance of model based controllers during large disturbance conditions. A numerically stable method of treating boundary conditions was also not included in the study. Kessal (2000) made use of an explicit finite difference method for time and spacial discretization in order to model slow transients in a gas pipeline. The slow transient consideration however cannot capture fast transient disturbances such as well or safety valve trip conditions. Chaczykowski and Zarodkiewicz (2017) developed a pipeline network model by making use of an implicit FDM in both time and space. Koo (2022) made use of an implicite FVM and an implicit MOC approach to solve the hyperbolic partial differential equations. However, implicit methods are not ideal for model based control applications due to the time required to recursively solve the resulting difference equations. Bermúdez and Shabani (2019) made use of the FEM to model a gas pipeline network. This method has advantages over the FDM approach as it has a higher accuracy and allows for the use of larger spacial and time discretization steps while maintaining numerical stability (Bermúdez and Shabani, 2019).

The SEM combines the versatility of the FDM and the accuracy of the FEM by implementing a spectral method on a spatially discretized section of the pipeline. The work in (Mennemann et al., 2018) made use of the SEM to develop a dynamic model of a pipeline for an incompressible fluid while the work in (Wiid et al., 2020) extended this model to a compressible fluid with non-constant values for the compressibility factor, molecular weight, gas viscosity, and pipe friction factor. The SEM shall be used to develop the model of the gas pipelines in the network due to its numerical stability, high accuracy and computational efficiency when compared to other methods. The nomenclature used in the model development is given in Table 2.1.

Table 2.1. Nomenclature.

Symbol	Description	Units
A	Pipe cross sectional area	m^2
C_v	Choke valve flow coefficient	-
C_w	Well deliverability coefficient	-
D	Pipe internal diameter	m
f	Pipe friction factor	-
l	Choke valve open command	-
L	Pipe length	m
M_w	Gas molar weight	kg/mol
P	Pressure	Pa
P_C	Critical pressure	Pa
P_e	Reservoir pressure	Pa
P_{TH}	Well tubing head pressure	Pa
q	Gas flow rate	kg/s
R	Gas constant	m^3 Pa $Kmol^{-1}$
Re	Reynolds number	-
T	Temperature	K
T_C	Critical temperature	K
u	Gas velocity	m/s
Z	Gas compressibility factor	-
ρ	Gas density	kg/m^3
ρ_C	Critical gas density	kg/m^3
η	Gas viscosity	Pa.s
ε	Pipe roughness	m

2.3 SINGLE PIPELINE GAS FLOW GOVERNING EQUATIONS

Gas flow dynamics in a gas pipeline is governed by a continuity (2.1) and momentum equation (2.2) (Fang et al., 2018). These equations are given by,

$$0 = \frac{\partial \rho}{\partial t} + \frac{\partial (\rho u)}{\partial z}, \tag{2.1}$$

$$0 = \frac{\partial P}{\partial z} + \frac{\partial (\rho u)}{\partial t} + \frac{\partial (\rho u^2)}{\partial z} + \frac{f \rho u^2}{2D}, \tag{2.2}$$

where ρ is the gas density, P is the gas pressure, u is the gas velocity, t is the time instant, z is the position along the pipeline, and f is the pipe friction factor. Equations (2.1) and (2.2) can be converted into an equation based on mass flow rate and pressure instead of density and velocity. This conversion is required because online density measurements for gas streams are not readily available in process plants. The conversion is based on the ideal gas equation (2.3) and the velocity to mass flow rate conversion equation (2.4). These equations are,

$$PM_w = \rho ZRT, \tag{2.3}$$

$$q = A \rho u, \tag{2.4}$$

where M_w is the molecular weight of the gas, Z is the compressibility factor of the gas, R is the gas constant, A is the cross sectional area of the gas pipeline and T is the gas temperature.

The continuity and momentum equations with mass flow rate and pressure as the conserved variables are,

$$0 = \frac{\partial P}{\partial t} + \frac{c^2}{A} \frac{\partial q}{\partial z}, \tag{2.5}$$

$$0 = \frac{\partial q}{\partial t} + A \frac{\partial P}{\partial z} + \frac{f c^2}{2AD} \frac{q^2}{P}, \tag{2.6}$$

where,

$$c = \sqrt{\frac{ZRT}{M_w}}, \tag{2.7}$$

is the speed of sound in the gas medium.

The third term in the momentum equation (2.2) is assumed to be negligible when converting (2.2) to (2.6). This assumption is valid because the gas flow velocities are much lower than the speed of sound (c) (Fang et al., 2018). The gas temperature T is assumed constant along the pipeline as the gas pipes are buried and insulated pipelines with a small difference of at most 20°C between the gas and ambient temperature. In addition, there are no compressors in the network which could result in temperature changes. It should be noted that (2.5) and (2.6) are only applicable for gas flow in one direction and do

not account for reverse flow. However, the one directional flow model is valid as the network being considered in the study is a production network where reverse flow is prevented in the system design even under abnormal conditions through the use of check valves.

2.4 SPATIAL DISCRETIZATION USING THE SEM

The gas pipeline models shown in (2.5) and (2.6) are continuous in both time and space. These equations have to be converted into a space discrete (state-space) form before they can be used in model based control applications. This section presents the method used to convert the continuous time and space equations into an accurate discrete space form.

2.4.1 Weak Formulation of the Pipeline Model

The SEM is used to implement spacial discretization in each pipeline of the production network. It is applied by first writing (2.5) and (2.6) in conservative matrix form as,

$$0 = \frac{\partial}{\partial t}\begin{bmatrix} P \\ q \end{bmatrix} + \begin{bmatrix} 0 & \frac{c^2}{A} \\ A & 0 \end{bmatrix} \frac{\partial}{\partial z}\begin{bmatrix} P \\ q \end{bmatrix} + \begin{bmatrix} 0 \\ \frac{fc^2}{2AD}\frac{q^2}{P} \end{bmatrix}. \tag{2.8}$$

Equation (2.8) is then converted into the form,

$$0 = \frac{\partial}{\partial t}\begin{bmatrix} \varepsilon P \\ \mu q \end{bmatrix} + \frac{\partial}{\partial z}\left(\begin{bmatrix} 0 & \frac{1}{\mu} \\ \frac{1}{\varepsilon} & 0 \end{bmatrix}\begin{bmatrix} \varepsilon P \\ \mu q \end{bmatrix}\right) + \begin{bmatrix} 0 \\ r\Theta(P,q) \end{bmatrix}, \tag{2.9}$$

where $\varepsilon = \frac{A}{c^2}$, $\mu = \frac{1}{A}$, $r = \frac{\mu f c^2}{2AD}$, $\Theta(P,q) = \frac{q^2}{P}$, and D is the gas pipeline diameter.

The SEM makes use of a weak formulation of the differential equation shown in (2.9), which is used to calculate an estimate of the spatial solution. A class of test functions v are chosen in order to implement the estimate as an integral of weighted residuals (Canuto et al., 2006). Therefore, the weak formulation is implemented by multiplying (2.9) by the test functions v and then integrating over the spatial domain $[0,L]$. The weak formulation is given by (Mennemann et al., 2018),

$$\int_0^L \left(\frac{\partial}{\partial t}\begin{bmatrix} \varepsilon P \\ \mu q \end{bmatrix} + \frac{\partial}{\partial z}\left(\begin{bmatrix} 0 & \frac{1}{\mu} \\ \frac{1}{\varepsilon} & 0 \end{bmatrix}\begin{bmatrix} \varepsilon P \\ \mu q \end{bmatrix}\right) + \begin{bmatrix} 0 \\ r\Theta \end{bmatrix}\right) v dz = 0. \tag{2.10}$$

Applying integration by parts on (2.10) results in,

$$\int_0^L \frac{\partial}{\partial t}\begin{bmatrix} \varepsilon P \\ \mu q \end{bmatrix} v dz = \int_0^L \begin{bmatrix} q \\ P \end{bmatrix} \frac{\partial v}{\partial z} dz - \int_0^L r \begin{bmatrix} 0 \\ \Theta \end{bmatrix} v dz + \mathbf{F}^*(0,t)v(0) - \mathbf{F}^*(L,t)v(L), \tag{2.11}$$

where $\mathbf{F}^*(z,t) = [F_1^*(z,t), F_2^*(z,t)]^T$ is the flux evaluated at spatial location z and time t.

2.4.2 Solution Approximation using Global Basis Functions

A polynomial approximation of the solution of (2.11) is given by,

$$P(z,t) \approx P_h(z,t) = \sum_{j=1}^{J} P_j(t)\phi_j(z), \tag{2.12}$$

$$q(z,t) \approx q_h(z,t) = \sum_{j=1}^{J} q_j(t)\phi_j(z). \tag{2.13}$$

The non-linear term $\Theta(P,q)$ in (2.9) is approximated as,

$$\Theta(z,t) \approx \Theta_h(z,t) = \sum_{j=1}^{J} \Theta_j(t)\phi_j(z). \tag{2.14}$$

The polynomial approximation of the solution of (2.11) makes use of a global basis functions $\phi_j(z)$. The global basis functions are defined in order to provide an exact solution for (2.11) at spacial points z_j.

2.4.3 Definition of Global Basis Functions

The global basis functions are created by making use of elemental basis functions. These elemental basis functions can be defined over the entire pipe length resulting in a FEM. However in the SEM approach, the elemental basis functions are defined in M discrete pipe segments. In this method the pipe spacial domain $\Omega = [0,L]$ is divided into M elements Z_m such that,

$$\Omega = \bigcup_{m=1}^{M} Z_m, \tag{2.15}$$

where $Z_m = [\bar{z}_{m-1}, \bar{z}_m]$ for $m = 1,2,\ldots,M-1,M$. The element edges satisfy $\bar{z}_0 = 0 < \bar{z}_1 < \ldots < \bar{z}_{M-1} < \bar{z}_M = L$ (Mennemann et al., 2018). The pipe spacial discretization is shown in Figure 2.1.

In each discretized spacial domain Z_m elemental basis functions $\varphi_i^m(z)$ are defined. The spectral method makes use of the characteristic Lagrange polynomials as the element basis functions. The characteristic Lagrange polynomials of degree N_m in the reference domain $\hat{\Omega} = [-1,1]$ are given by

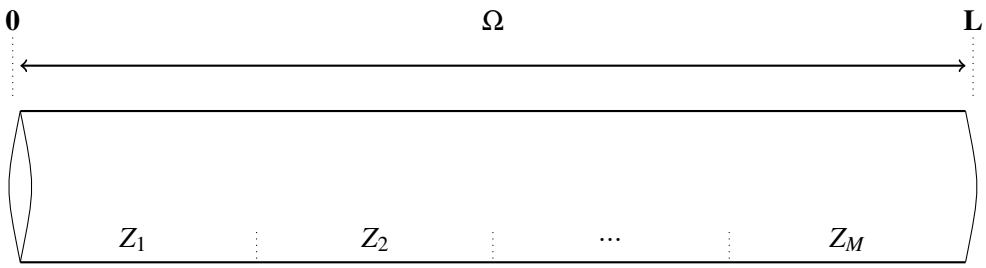

Figure 2.1. Pipe Spacial Discretization for the SEM.

(Canuto et al., 2007),

$$\varphi_i^{(m)}(\varepsilon) = \frac{\frac{\lambda_i}{\varepsilon-\varepsilon_i}}{\sum_{k=0}^{N_m} \frac{\lambda_k}{\varepsilon-\varepsilon_k}}, \tag{2.16}$$

where,

$$\lambda_i = \frac{1}{\prod_{k\neq i}(\varepsilon_i - \varepsilon_k)}, \tag{2.17}$$

for $i = 0, 1, \ldots, N_m$ and $\varepsilon \in \hat{\Omega}$.

These polynomials up to degree 4 are shown in Figure 2.2. From Figure 2.2 it can be noted that the polynomial functions are orthogonal at points $\varepsilon = -1$, $\varepsilon = -0.4$, $\varepsilon = 0.4$ and $\varepsilon = 1$. Therefore, the sum of the polynomial functions can provide an exact estimate of a function value at these points.

The form of the characteristic Lagrange polynomials in (2.16) is called the Barycentric form and is more numerically stable as compared to the standard form (Canuto et al., 2007). The points or nodes $\varepsilon_0, \varepsilon_1, .., \varepsilon_{N_m}$ are the Legendre-Gauss-Lobatto (LGL) nodes and are calculated as the zeros of $(1-\varepsilon^2)P'_{N_m}$ where P_{N_m} is the characteristic Legendre polynomial of order N_m and P'_{N_m} is the first derivative of the characteristic Legendre polynomial with respect to ε. The characteristic Legendre polynomials can be calculated by making use of a recursive equation as:

$$P_{N_m+1}(x) = \frac{2N_m+1}{N_m+1} x, P_{N_m}(x) - \frac{N_m}{N_m+1} P_{N_m-1}(x), \tag{2.18}$$

where,

$$P_0(x) = 1 \text{ and } P_1(x) = x. \tag{2.19}$$

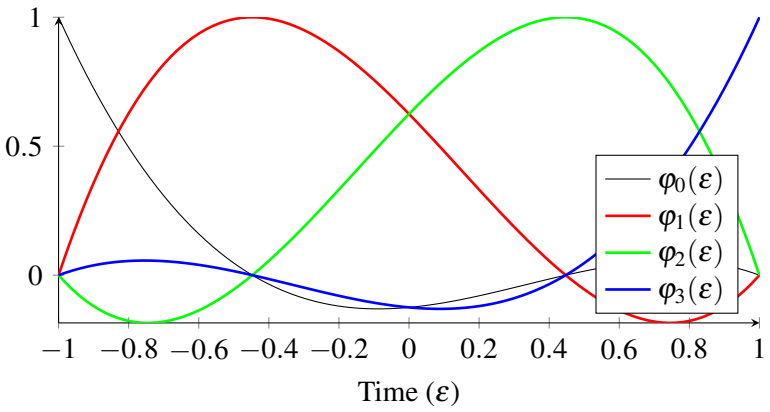

Figure 2.2. Basis functions (Lagrange polynomials) for $N_m = 3$.

The elemental basis functions are mapped from the reference domain $\hat{\Omega}$ to the spatial element domain Z_m by making use of the transform,

$$\Gamma_m(\varepsilon) = z_m = \frac{\bar{z}_m - \bar{z}_{m-1}}{2}\varepsilon + \frac{\bar{z}_m + \bar{z}_{m-1}}{2}. \tag{2.20}$$

The transformation in (2.20) is used to define the elemental basis function in the spatial domain $z \in [\bar{z}_{m-1}, \bar{z}_m]$ as (Canuto et al., 2007; Mennemann et al., 2018),

$$\varphi_i^m(z) = \varphi_i^m(\Gamma_m^{-1}(z)). \tag{2.21}$$

The element basis functions are combined to create global basis functions $\phi_j(z)$ which are continuous over the spatial interval $z \in [0, L]$ for $j = 1, 2, \ldots \sum N_m + 1$. Element basis function i in element m corresponds to global basis function $j = (N_m - 1)(m-1) + i$. In forming global basis function j, element basis function i in domain m is extended to cover the domain of the global basis function as described below,

$$\phi_j(z) = \begin{cases} \varphi_i^m(z) & \text{for } z \in Z_m \\ 0 & \text{otherwise.} \end{cases} \tag{2.22}$$

Special consideration has to be taken for the case when $i = 0$ and $i = N_m$ in order to ensure that the global basis function is smooth and does not have discontinuities. The element basis functions for these cases are converted into global basis functions by joining element basis functions φ_0^{m+1} and $\varphi_{N_m}^m$ as (Canuto et al., 2007),

$$\phi_j(z) = \begin{cases} \varphi_{N_m}^m(z) & \text{for } z \in Z_m \\ \varphi_0^m(z) & \text{for } z \in Z_{m+1} \\ 0 & \text{otherwise.} \end{cases} \tag{2.23}$$

2.4.4 Weak Formulation Solution

The SEM used in this study is a Galerkin method. This is a spectral method in which the form of the global basis functions are the same as the test functions (Canuto et al., 2006). Therefore, the test functions are given by $\phi_i(z)$.

The weak formulation in (2.11) is solved by substituting the polynomial approximations of $P(z,t)$, $q(z,t)$ and $\Theta(z,t)$ into (2.11). $\phi_i(z)$ is substituted in place of the test functions. The weak formulation

for (2.11) is therefore,

$$\frac{\partial P_1(t)}{\partial t}\int_0^L \varepsilon\phi_1(z)\phi_i(z)dz+\ldots+\frac{\partial P_J(t)}{\partial t}\int_0^L \varepsilon\phi_J(z)\phi_i(z)dz = q_1(t)\int_0^L \phi_1(z)\frac{\partial\phi_i(z)}{\partial z}dz+\ldots+q_J(t)\int_0^L \phi_J(z)\frac{\partial\phi_i(z)}{\partial z}dz + q^*(0,t)\phi_i(0)-q^*(L,t)\phi_i(L), \quad (2.24)$$

and,

$$\frac{\partial q_1(t)}{\partial t}\int_0^L \mu\phi_1(z)\phi_i(z)dz+\ldots+\frac{\partial q_J(t)}{\partial t}\int_0^L \mu\phi_J(z)\phi_i(z)dz = P_1(t)\int_0^L \phi_1(z)\frac{\partial\phi_i(z)}{\partial z}dz+\ldots+P_J(t)\int_0^L \phi_J(z)\frac{\partial\phi_i(z)}{\partial z}dz - \left[\Theta_1(t)\int_0^L r\phi_1(z)\phi_i(z)dz+\ldots+\Theta_J(t)\int_0^L r\phi_J(z)\phi_i(z)dz\right] + P^*(0,t)\phi_i(0)-P^*(L,t)\phi_i(L). \quad (2.25)$$

Equations (2.24) and (2.25) can be written in matrix form by defining,

$$S_{i,j}=\int_0^L \phi_j(z)\frac{\partial\phi_i(z)}{\partial z}dz, \quad (2.26)$$

$$(M_x)_{i,j}=\int_0^L x(z)\phi_j(z)\phi_i(z)dz, \quad (2.27)$$

where $S_{i,j}$ is the stiffness matrix value for test function i and node j, and $(M_x)_{i,j}$ is the mass matrix value for test function i and node j. The row position in the matrices is i and the column position is j. The resulting matrix form of the weak formulation solution is (Mennemann et al., 2018),

$$\mathbf{M}_\varepsilon\frac{\partial\mathbf{P}}{\partial t}=\mathbf{Sq}+q_1^*\mathbf{e_1}-q_J^*\mathbf{e_J}, \quad (2.28)$$

$$\mathbf{M}_\mu\frac{\partial\mathbf{q}}{\partial t}=\mathbf{SP}-\mathbf{M}_r\mathbf{\Theta}+P_1^*\mathbf{e_1}-P_J^*\mathbf{e_J}, \quad (2.29)$$

where $\mathbf{P}=[P_1,P_2,\ldots,P_J]^T$, $\mathbf{q}=[q_1,q_2,\ldots,q_J]^T$, $\mathbf{\Phi}=[\Theta_1,\Theta_2,\ldots,\Theta_J]^T$, $\mathbf{e_1}=[1,0,0,0,\ldots,0]^T$ and $\mathbf{e_J}=[0,0,\ldots,1]^T$.

It can be noted that (2.28) and (2.29) are in discrete space or state-space form as required. Equations (2.28) and (2.29) can be written in traditional state-space form as,

$$\frac{\partial\mathbf{x}}{\partial t}=\mathbf{f}(\mathbf{x},q_1^*,q_J^*,P_1^*,P_J^*), \quad (2.30)$$

$$=\begin{bmatrix}\mathbf{M}_\varepsilon^{-1}\left(\mathbf{Sq}+q_1^*\mathbf{e_1}-q_J^*\mathbf{e_J}\right)\\ \mathbf{M}_\mu^{-1}\left(\mathbf{SP}-\mathbf{M}_r\mathbf{\Theta}+P_1^*\mathbf{e_1}-P_J^*\mathbf{e_J}\right)\end{bmatrix}, \quad (2.31)$$

where $\mathbf{x} = [\mathbf{P}, \mathbf{q}]^T$. Equation (2.30) shows that the flux values of pressure (P^*) and flow (q^*) at each pipeline boundary acts as the inputs or forcing function for each pipeline state space model. The use of flux values instead of boundary pressures and flows as the pipeline model forcing functions results in the improved stability of the SEM.

Equation (2.8) shows that the model results are dependent on the gas temperature due to parameter c. This means that a significant change in temperature along the pipeline will have an effect on the pressure and flow transients therefore leading to model prediction errors. It should be noted that conversion of (2.25) and (2.24) into (2.28) and (2.29) respectively is still valid under conditions where parameters μ, ε, r and consequently c vary along the pipeline. This means that the model can be extended to cases where there is a temperature or composition change along the pipeline by incorporating a mathematical model of the temperature or composition to the developed pipeline model.

2.4.5 Mass and Stiffness Matrix Calculation

The solution of the mass and stiffness matrices is based on the quadrature formula of Canuto et al. (2006), such that,

$$\int_{-1}^{1} p(\varepsilon)d\varepsilon = \sum_{j=0}^{N_m} p(\varepsilon_j)w_j, \tag{2.32}$$

where w_j is the integration weight. For the LGL nodes the integration weights are calculated by,

$$w_j = \frac{2}{N_m(N_m+1)[P_{N_m}(\varepsilon_j)]^2}. \tag{2.33}$$

The quadrature formula can be transformed from the reference domain $\hat{\Omega}$ to the spatial domain by making use of transform (2.20). The resulting quadrature formula is,

$$\int_{\bar{z}_{m-1}}^{\bar{z}_m} p(z)dz = \frac{h}{2}\sum_{j=0}^{N_m} p(z)w_j, \tag{2.34}$$

where $h = \bar{z}_m - \bar{z}_{m-1}$. The same spatial discretization length (h) shall be assumed in each element. Therefore, the elements of the mass and stiffness matrices are,

$$\begin{aligned}(M_x)_{i,j} &= \int_0^L x(z)\phi_j(z)\phi_i(z)dz \\ &= \frac{h}{2}\sum_{k=1}^{J} x(z_k)\phi_j(z_k)\phi_i(z_k)w_k \\ &= \begin{cases} \frac{h}{2}x(z_i)w_i & \text{for } i=j=k \\ 0 & \text{otherwise} \end{cases},\end{aligned} \tag{2.35}$$

$$\begin{aligned} S_{i,j} &= \int_0^L \phi_j(z) \frac{\partial \phi_i(z)}{\partial z} dz \\ &= \sum_{k=1}^{J} \phi_j(z_k) \frac{\partial \phi_i(z_k)}{\partial z} w_k \\ &= \frac{\partial \phi_i(z_j)}{\partial z} w_j. \end{aligned} \tag{2.36}$$

The derivative of the test function in (2.36) is calculated by (Canuto et al., 2007),

$$\begin{aligned} \frac{\partial \phi_i(z_k)}{\partial z} &= \sum_{l=0}^{N} (D_N)_{k,l} \phi_i(z_l) \\ &= (D_N)_{j,i} w_j, \end{aligned} \tag{2.37}$$

where,

$$(D_N)_{k,l} = \begin{cases} \frac{P_N(z_k)}{P_N(z_l)} \frac{1}{z_k - z_l} & \text{for } k \neq l \\ \frac{-(N+1)N}{4} & \text{for } k = l = 0 \\ \frac{N(N+1)}{4} & \text{for } k = l = N \\ 0 & \text{otherwise.} \end{cases} \tag{2.38}$$

2.5 STATE-SPACE MODEL TIME DISCRETIZATION

The discrete-space model (2.30) is discretized in time by making use of the 4th order Runge-Kutta discretization method with a fixed time step (T_s). Given known state parameters at time $t = t_n$ given by $\mathbf{x}_n$, the state parameters at the next time instant $t = t_n + Ts$ are given by (Canuto et al., 2007; Guedes et al., 2024),

$$\mathbf{k}_1 = \mathbf{f}(\mathbf{x}_n, q^*_{1,n}, q^*_{J,n}, P^*_{1,n}, q^*_{J,n}) \tag{2.39}$$

$$\mathbf{k}_2 = \mathbf{f}(\mathbf{x}_n + \frac{T_s}{2}\mathbf{k}_1, q^*_{1,n}, q^*_{J,n}, P^*_{1,n}, q^*_{J,n}) \tag{2.40}$$

$$\mathbf{k}_3 = \mathbf{f}(\mathbf{x}_n + \frac{T_s}{2}\mathbf{k}_2, q^*_{1,n}, q^*_{J,n}, P^*_{1,n}, q^*_{J,n}) \tag{2.41}$$

$$\mathbf{k}_4 = \mathbf{f}(\mathbf{x}_n + T_s\mathbf{k}_3, q^*_{1,n}, q^*_{J,n}, P^*_{1,n}, q^*_{J,n}) \tag{2.42}$$

$$\mathbf{x}_{n+1} = \mathbf{x}_n + \frac{1}{6}T_s(\mathbf{k}_1 + 2\mathbf{k}_2 + 2\mathbf{k}_3 + \mathbf{k}_4). \tag{2.43}$$

2.6 BOUNDARY CONDITIONS

The choice of boundary conditions for the hyperbolic system shown in (2.9) can have a significant influence on the stability of the solution. A stable method of enforcing boundary conditions is the characteristic compatibility method (CCM) (Canuto et al., 2007). The CCM method is implemented by first writing (2.9) in compact form as,

$$\frac{\partial \mathbf{U}}{\partial t} + \mathbf{A}\frac{\partial \mathbf{U}}{\partial z} + f(\mathbf{U}) = 0, \tag{2.44}$$

where $\mathbf{U}$ is a vector containing the physical variables of flow rate and pressure. $\mathbf{U}$ is converted into characteristic variables $\mathbf{Z}$ that travels in only one wave direction by,

$$\mathbf{Z} = \mathbf{W}^{-1}\mathbf{U}, \tag{2.45}$$

where $\mathbf{W}$ is the eigenvector matrix of parameter $\mathbf{A}$ in (2.44).

The CCM method is implemented at each boundary by expressing the incoming characteristic variables at the boundary in terms of the outgoing characteristic variables and boundary data. Variables used in the boundary condition calculations are shown in Figure 2.3. The boundary condition at the pipe inlet ($z = 0$) is given by $\mathbf{g_L}(0,t)$ and the boundary condition at the pipe outlet ($z = L$) is given by $\mathbf{g_R}(L,t)$. $\mathbf{Z}^-(0,t)$ is the characteristic variable propagated from the pipe interior towards the pipe inlet boundary while $\mathbf{Z}^+(0,t)$ is the characteristic variable propagated from the inlet boundary towards the pipe interior. $\mathbf{Z}^-(L,t)$ is the characteristic variable propagated from the pipe outlet boundary towards the pipe interior while $\mathbf{Z}^+(L,t)$ is the characteristic variable propagated from the pipe interior towards the pipe outlet boundary.

2.6.1 Boundary Condition Implementation at the Pipe Inlet

Boundary conditions at the pipe inlet are written in terms of the physical and characteristic variables as,

$$\mathbf{B_L}\mathbf{U}(0,t) = \mathbf{g_L}(0,t), \tag{2.46}$$

$$\mathbf{C_L}\mathbf{Z}(0,t) = \mathbf{g_L}(0,t), \tag{2.47}$$

$$\mathbf{C_L}^+\mathbf{Z}^+(0,t) + \mathbf{C_L}^-\mathbf{Z}^-(0,t) = \mathbf{g_L}(0,t), \tag{2.48}$$

where,

$$\mathbf{C_L} = \mathbf{B_L}\mathbf{W_L}, \tag{2.49}$$

and $\mathbf{B_L}$ is a matrix that relates the boundary constraint $\mathbf{g_L}(0,t)$ to the physical variables $\mathbf{U}$. The expression for the incoming characteristic ($\mathbf{Z}^+$) at the inlet boundary can be derived from (2.48)

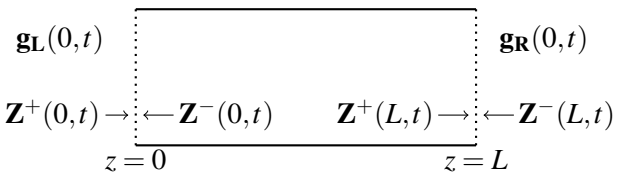

Figure 2.3. Variables used in calculating boundary conditions where the left hand side is the inlet and the right hand side is the outlet of the pipe.

resulting in,

$$\mathbf{Z}^{+}(0,t) = \mathbf{S_L}\mathbf{Z}^{-}(0,t) + \mathbf{Z_L}(\mathbf{t}), \tag{2.50}$$

where,

$$\mathbf{S_L} = -(\mathbf{C_L}^{+})^{-1}\mathbf{C_L}^{-}, \tag{2.51}$$

$$\mathbf{Z_L}(t) = (\mathbf{C_L}^{+})^{-1}\mathbf{g_L}(t). \tag{2.52}$$

Since $\mathbf{Z}^{-}(0,t)$ is the characteristic variable that is propagated from the interior, it can be expressed as,

$$\mathbf{Z}^{-}(0,t) = (\mathbf{W}^{-})^{-1}\begin{bmatrix} P_1 \\ q_1 \end{bmatrix}. \tag{2.53}$$

2.6.2 Boundary Condition Implementation at the Pipe Outlet

Boundary conditions at the pipe outlet are written in terms of the physical and characteristic variables as,

$$\mathbf{B_R}\mathbf{U}(L,t) = \mathbf{g_R}(L,t), \tag{2.54}$$

$$\mathbf{C_R}\mathbf{Z}(L,t) = \mathbf{g_R}(L,t), \tag{2.55}$$

$$\mathbf{C_R}^{+}\mathbf{Z}^{+}(L,t) + \mathbf{C_R}^{-}\mathbf{Z}^{-}(L,t) = \mathbf{g_R}(L,t), \tag{2.56}$$

where,

$$\mathbf{C_R} = \mathbf{B_R}\mathbf{W_R}, \tag{2.57}$$

and $\mathbf{B_R}$ is a matrix that relates the boundary constraint $\mathbf{g_R}(L,t)$ to the physical variables $\mathbf{U}$.

The expression for the incoming characteristic ($\mathbf{Z}^{-}$) at the outlet boundary is given by,

$$\mathbf{Z}^{-}(L,t) = \mathbf{S_R}\mathbf{Z}^{+}(L,t) + \mathbf{Z_R}(\mathbf{t}), \tag{2.58}$$

where,

$$\mathbf{S_R} = -(\mathbf{C_R}^{-})^{-1}\mathbf{C_R}^{+}, \tag{2.59}$$

$$\mathbf{Z_R}(t) = (\mathbf{C_R}^{-})^{-1}\mathbf{g_R}(t). \tag{2.60}$$

Since $\mathbf{Z}^{+}(L,t)$ is the characteristic variable that is propagated from the interior, it can be expressed as,

$$\mathbf{Z}^{+}(L,t) = (\mathbf{W}^{+})^{-1}\begin{bmatrix} P_J \\ q_J \end{bmatrix}. \tag{2.61}$$

2.6.3 Application of the CCM Method to Calculate Boundary Conditions

The CCM method is used to calculate the values of $\mathbf{F}^*(0,t)$ and $\mathbf{F}^*(L,t)$ in (2.11) as shown below.

$$\begin{aligned}\mathbf{F}^*(0,t) &= \mathbf{A}\mathbf{U}(0,t) = \mathbf{W}\boldsymbol{\Lambda}\mathbf{Z}(0,t)\\ &= \mathbf{W}^+\boldsymbol{\Lambda}^+\mathbf{Z}^+(0,t) + \mathbf{W}^-\boldsymbol{\Lambda}^-\mathbf{Z}^-(0,t) \qquad (2.62)\\ \mathbf{F}^*(L,t) &= \mathbf{A}\mathbf{U}(L,t) = \mathbf{W}\boldsymbol{\Lambda}\mathbf{Z}(L,t)\\ &= \mathbf{W}^+\boldsymbol{\Lambda}^+\mathbf{Z}^+(L,t) + \mathbf{W}^-\boldsymbol{\Lambda}^-\mathbf{Z}^-(L,t) \qquad (2.63)\end{aligned}$$

The expression for the incoming characteristic at the inlet boundary is substituted into (2.62) resulting in,

$$\mathbf{F}^*(0,t) = (\mathbf{W}^+\boldsymbol{\Lambda}^+\mathbf{S_L} + \mathbf{W}^-\boldsymbol{\Lambda}^-)(\mathbf{W}^-)^{-1}\begin{bmatrix}P_1\\ q_1\end{bmatrix} + \mathbf{W}^+\boldsymbol{\Lambda}^+(\mathbf{C_L}^+)^{-1}\mathbf{g_L}(t). \qquad (2.64)$$

Similarly, the expression for the incoming characteristic at the outlet boundary is substituted into (2.63) resulting in,

$$\mathbf{F}^*(L,t) = (\mathbf{W}^+\boldsymbol{\Lambda}^+ + \mathbf{W}^-\boldsymbol{\Lambda}^-\mathbf{S_R})(\mathbf{W}^+)^{-1}\begin{bmatrix}P_J\\ q_J\end{bmatrix} + \mathbf{W}^-\boldsymbol{\Lambda}^-(\mathbf{C_R}^-)^{-1}\mathbf{g_R}(t), \qquad (2.65)$$

2.7 ESTIMATION OF SINGLE PIPELINE MODEL UNKNOWN PARAMETERS

The unknown parameters in the single pipeline model are the gas compressibility factor (Z) and pipeline friction factor (f). The pipeline model parameters are calculated from first principles using the equations described in this section. The gas molar weight (M_w) is assumed to be constant and known over the entire gas field. It should be noted that the developed model is independent of the network operating conditions due to all pipeline model parameters being calculated from first principles instead of being estimated from operating data.

2.7.1 Gas Compressibility Factor

The compressibility factor (Z) of a natural gas stream is traditionally calculated by making use of Equations of State (EOS) such as the Peng Robinson EOS (Peng and Robinson, 1976), Soave-Redlich-Kwong EOS (Soave, 1972) and the AGA-8 Detail Characterization Method (Starling and Savidge, 1994). These methods require a recursive computation to calculate the value of Z which is undesired for model based control applications. An explicit correlation is more applicable for such time and computational resource constrained applications such as the method proposed by Kareem et al. (2016). Therefore, the compressibility factor in this study is calculated using an explicit correlation method given by (Ekechukwu and Orodu, 2019; Kareem et al., 2016),

$$Z = \frac{DP_{Pr}(1+Y+Y^2-Y^3)}{(DP_{Pr}+EY^2-FY^G)(1-Y)^3}, \tag{2.66}$$

where,

$$Y = \frac{DP_{Pr}}{\frac{a+A^2}{C} - \frac{A^2B}{C^3}},$$

and parameters A, B, C, D, E, F and G are given by expressions (Kareem et al., 2016),

$$A = \frac{a_1}{T_{Pr}} e^{a_2(1-\frac{1}{T_{Pr}})^2} P_r,$$

$$B = \frac{a_3}{T_{Pr}} + \frac{a_4}{{T_{Pr}}^2} + a_5\left(\frac{P_{Pr}}{T_{Pr}}\right)^6,$$

$$C = a_9 + a_8\frac{P_{Pr}}{T_{Pr}} + a_7\left(\frac{P_{Pr}}{T_{Pr}}\right)^2 + a_6\left(\frac{P_{Pr}}{T_{Pr}}\right)^3,$$

$$D = \frac{a_{10}}{T_{Pr}} e^{a_{11}(1-\frac{1}{T_{Pr}})^2},$$

$$E = \frac{a_{12}}{T_{Pr}} + \frac{a_{13}}{{T_{Pr}}^2} + \frac{a_{14}}{{T_{Pr}}^3},$$

$$F = \frac{a_{15}}{T_{Pr}} + \frac{a_{16}}{{T_{Pr}}^2} + \frac{a_{17}}{{T_{Pr}}^3},$$

$$G = a_{18} + \frac{a_{19}}{T_{Pr}}.$$

Constants a_i in the explicit correlation expressions are shown in Table 2.2.

The pseudo-reduced pressure (P_{Pr}) and pseudo-reduced temperature (T_{Pr}) in (2.66) are given by $P_{Pr} = \frac{P}{P_C}$ and $T_{Pr} = \frac{T}{T_C}$ where P_C is the pseudo-critical pressure and T_C is the pseudo-critical temperature. The pseudo-critical temperature and pseudo-reduced pressures are calculated based knowledge of the gas composition. P_C is given by,

$$P_C = \sum_i y_i P_{Ci}, \tag{2.67}$$

where y_i is the mole fraction of the i-th component in the gas and P_{Ci} is the critical pressure of the i-th component. Similarly T_C is given by,

$$T_C = \sum_i y_i T_{Ci}. \tag{2.68}$$

Equation (2.66) is valid for $0.2 < P_{Pr} < 15$ and $1.15 < T_{Pr} < 3$ and was chosen for its low complexity and low estimation error in this range. It should be noted that these validity limits are applicable for gas production networks.

2.7.2 Coefficient of Friction

The friction factor (f) in a pipe can be calculated by making use of the Colebrook White equation (2.69). This equation is given by,

$$\frac{1}{\sqrt{f}} = -2\log\left(\frac{2.51}{Re\sqrt{f}} + \frac{\varepsilon/D}{3.71}\right), \tag{2.69}$$

where Re is the Reynolds number and ε is the pipe roughness. The Reynolds number is calculated by,

$$Re = \frac{\rho u L}{\eta}, \tag{2.70}$$

where η is the dynamic viscosity of the gas.

The Colebrook white equation can be used to calculate coefficients of friction in smooth and turbulent flow regimes. However, the equation is not suitable for control applications at it needs to be solved recursively which requires extensive computational resources. For control applications, an explicit friction factor correlation is required. A number of authors have proposed explicit estimates of the Colebrook white equation. The explicit friction factor correlation used in this study is given by

Table 2.2. Constants used in Compressibility factor Calculation.

Parameter	Value	Parameter	Value
a_1	0.317842	a_2	0.382216
a_3	-7.76835	a_4	14.2905
a_5	2.18363e-6	a_6	-0.00469257
a_7	0.0962541	a_8	0.16672
a_9	0.96691	a_{10}	0.063069
a_{11}	-1.966847	a_{12}	21.0581
a_{13}	-27.0246	a_{14}	16.23
a_{15}	207.783	a_{16}	-488.161
a_{17}	176.29	a_{18}	1.88453
a_{19}	3.05921		

(Zeghadnia et al., 2019; Vatankhah, 2014),

$$f = \left(\frac{2.51/Re + 1.1513\delta}{\delta - (\varepsilon/D) - 2.3026\delta \log \delta} \right)^2, \tag{2.71}$$

where,

$$\delta = \frac{6.0173}{Re(0.07(\varepsilon/D) + Re^{-0.885})^{0.109}} + \frac{\varepsilon/D}{3.71}. \tag{2.72}$$

The gas dynamic viscosity η is calculated as,

$$\eta = 0.0001 \times B\sqrt{T_{Pr}} \exp\left(\frac{\theta + (A_b + A_k T_{Pr})\rho_{Pr}^{\alpha}}{T_{Pr}} \right) \sum_{i=1}^{n} y_i \sqrt{M_i}. \tag{2.73}$$

The constants in (2.73) are given by $B = 3.142$, $\theta = -0.551$, $A_k = 0.172$, $A_b = 0.621$ and $\alpha = 1.273$ (Yang et al., 2017). The correlation in (2.71) is recommended by Zeghadnia et al. (2019) after comparisons with other explicit friction factor correlation methods such as the method of Romeo et al. (2002), Achour and Bedjaoui (2012), and Zigrang and Sylvester (1982).

2.8 GAS WELL DELIVERABILITY MODEL

A typical gas well is shown in Figure 2.4. The gas from the reservoir flows into the well driven by the differential pressure between the reservoir pressure P_e and pressure in the well outlet P_{TH}. The gas flow from the well can be modelled by (Wang and Economides, 2009; Smith, 1961),

$$q = C_w(P_e^2 - P_{TH}^2)^n, \tag{2.74}$$

where q is the rate of inflow of gas from the reservoir to the wellbore and n is a factor that is used to capture deviation of the well performance from the performance estimated from Darcy's law (Wang and Economides, 2009). This value has to be estimated for each well based on measured data. Parameter C_w is used to capture the pressure drop from the reservoir to the wellbore and is mainly affected by the reservoir permeability (Wang and Economides, 2009).

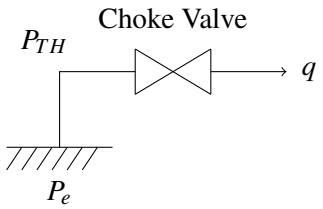

Figure 2.4. Typical gas well.

2.9 CHOKE VALVE MODEL

The gas flow from a well is controlled by making use of a choke valve. This is a specialized valve designed for the harsh conditions experienced in wellheads. Although detailed non-linear models of gas flow through choke valves are available (Bahadori, 2012; Nejatian et al., 2014), a simplified model as defined in ANSI/ISA-75.01.01 (International Society of Automation, 2007) will be used in this study in order to ensure reduced computational complexity. This model is given by,

$$q = C_v P_{TH} \sqrt{\frac{P_{TH} - P_0}{P_{TH} M_w T_{TH} Z}}, \tag{2.75}$$

where P_0 is the choke valve outlet pressure and Z is the choke valve inlet gas compressibility factor. The valve coefficient C_v is approximated as a third order polynomial given by (Grace and Frawley, 2011),

$$C_v = k_1 l^3 + k_2 l^2 + k_3 l + k_4, \tag{2.76}$$

where l is the fractional valve lift command.

2.10 CHAPTER CONCLUSION

Mathematical models for the components of a natural gas production network were developed in this chapter. The model of the natural gas pipeline network was developed as a discrete state-space model using the spectral element method (SEM). The model includes non-linear parameters such as the pipeline friction factors and gas compressibility factors by making use of explicit correlations. These non-linear parameters are assumed constant in most of the work presented in literature. A method of handling boundary conditions for the pipeline state-space model was also developed using the characteristic compatibility method. Steady-state models for the choke valve and natural gas wellheads were also developed and presented. The developed models will be combined through boundary conditions in Chapter 3 to obtain an overall natural gas production system model.

CHAPTER 3 MODELLING A NATURAL GAS NETWORK

This chapter aims to combine the gas pipeline, choke valve and gas well deliverability models presented in Chapter 2 in order to obtain a model of the complete natural gas production network. Section 3.1 presents a description of the natural gas supply and distribution network considered in this study. Section 3.2 presents the junction properties and boundary conditions applied to the ends of each pipeline in the network based on the CCM method described in Section 2.6. Section 3.2 also presents the developed overall system model in block diagram form. The method used to estimate the values of unknown parameters in this model is then defined in Section 3.3. Section 3.4 presents the spacial and time discretization step sizes required for a numerically stable and accurate solution.

3.1 NATURAL GAS SUPPLY AND DISTRIBUTION NETWORK DESCRIPTION

The natural gas production network that will be considered in this study is shown in Figure 3.1. This network is made up of 12 natural gas wells that feed into one header. The wells produce gas that is mainly composed of methane ($> 90\%$). The gas compositions in these wells are as shown in Loegering and Milkov (2017) for the Pande gas field. The main control objective in the network is to meet consumer gas demands. Therefore, the consumer battery limit pressure (P_{35}) is an important controlled variable (CV) as it is an indication of the gas demand (q_{35}) being met. The consumer gas demand (q_{35}) acts as a disturbance variable (DV) for the network. The manipulated variables (MVs) are the choke valve commands (l_i) of each well. The MVs are adjusted in order to set the gas flow rate (q_i) from each well (CVs) in an attempt to meet the gas demands. The network has a high limit on the network pressure (P_8) for safety considerations. This variable is also a CV in the network. All MVs, CVs and DVs in the network are shown in Figure 3.1.

3.2 NATURAL GAS NETWORK MODEL DEVELOPMENT

The gas distribution network model is developed from a state-space model of each pipeline in the network. These models are combined through appropriate junction properties and boundary conditions in order to obtain an overall system state-space model.

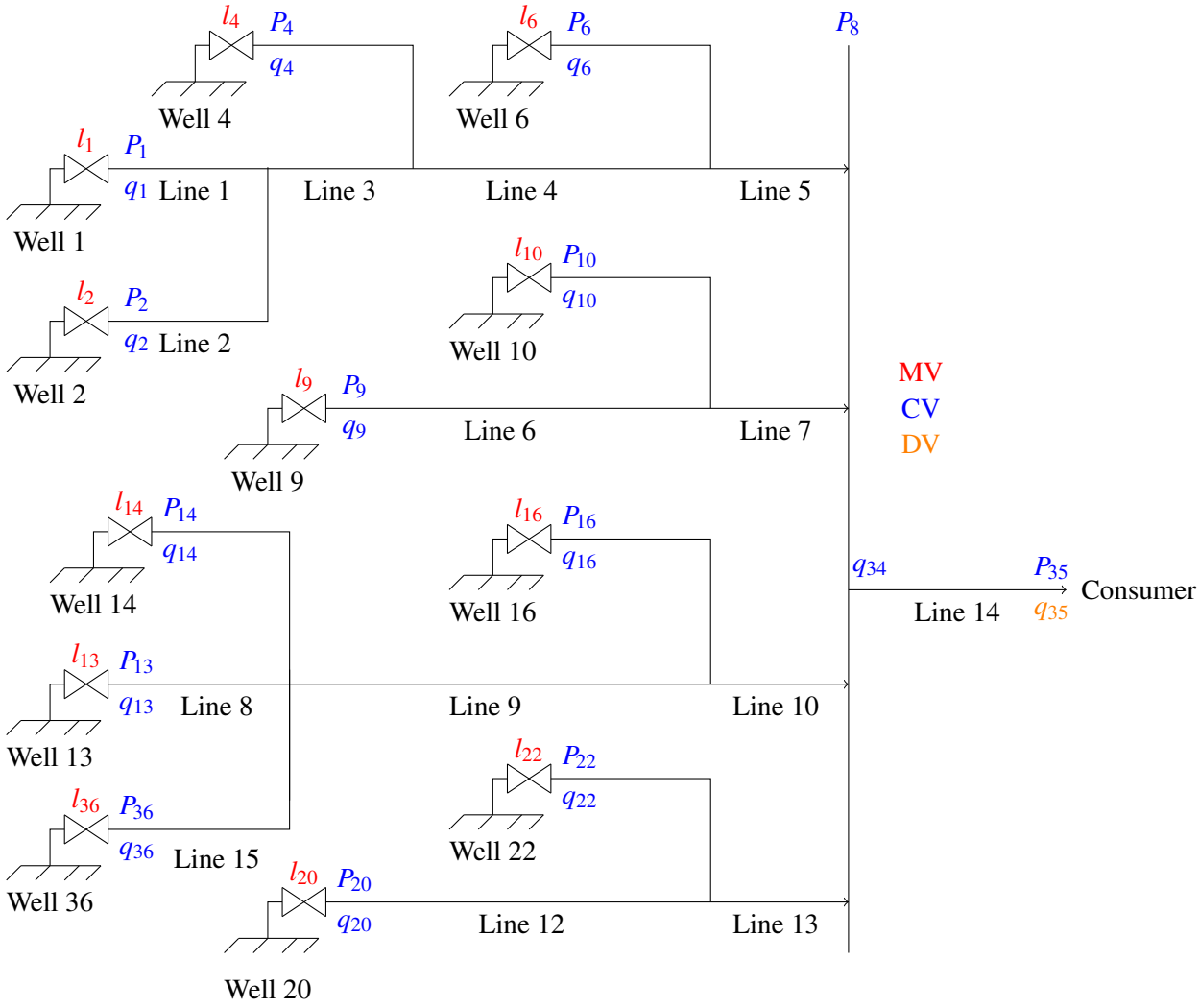

Figure 3.1. Industrial natural gas supply and distribution network showing MVs in red, CVs in blue and DVs in orange. It should be noted that pipelines of negligible length are not assigned line numbers, e.g., pipe from Well 22 to Line 13.

3.2.1 Junction Properties used to Combine Individual Pipeline State-Space Models

The first junction property used to combine individual pipeline models is the assumption that all pressures at a junction are equal, i.e.,

$$P_{J,i} = P_{1,n}, \tag{3.1}$$

where $P_{J,i}$ is the outlet pressure of the i-th pipeline connected to the junction and $P_{1,n}$ is the inlet pressure of the n-th pipeline connected to the junction.

The second junction property is the conservation of mass at each junction described by,

$$\sum_i q_{J,1} = \sum_n q_{1,n}, \tag{3.2}$$

where $q_{J,i}$ is the outlet flow of the i-th pipeline connected to the junction and $q_{1,n}$ is the inlet flow of the n-th pipeline connected to the junction.

3.2.2 Boundary Conditions for Individual Pipeline Models

Three types of distribution network pipelines will be considered in defining pipeline boundary conditions. These are,

- Pipelines connected to a gas well choke valve
- Pipelines connected to a junction
- Pipelines connecting consumers to a header

Applicable boundary conditions for these pipeline types are defined in the sections that follow.

3.2.2.1 Pipelines Connected to a Gas Well Choke Valve

The boundary conditions for pipelines connected to a gas well through a choke valve shall be the pipeline inlet pressure $P_0(t)$ and outlet pressure $P_L(t)$. The boundary conditions are therefore defined as,

$$\mathbf{B_L}\mathbf{U}(0,t) = g_L(t) = P_0(t), \tag{3.3}$$

$$\mathbf{B_R}\mathbf{U}(0,t) = g_R(t) = P_L(t). \tag{3.4}$$

Applying the CCM method to these boundary conditions results in,

$$\mathbf{F}^*(0,t) = \begin{bmatrix} q_1^*(t) \\ P_1^*(t) \end{bmatrix} = \begin{bmatrix} q_1(t) + \frac{A}{c}(P_0(t) - P_1(t)) \\ P_0(t) \end{bmatrix}, \tag{3.5}$$

$$\mathbf{F}^*(L,t) = \begin{bmatrix} q_J^*(t) \\ P_J^*(t) \end{bmatrix} = \begin{bmatrix} q_J(t) + \frac{A}{c}(P_J(t) - P_L(t)) \\ P_L(t) \end{bmatrix}, \tag{3.6}$$

where $P_L(t)$ is an input from the downstream pipeline and $P_0(t)$ is calculated by making use of the gas well deliverability model (2.74) and choke valve model (2.75). Application of (2.74) and (2.75) results in the equation for the inlet pressure being given by,

$$\begin{aligned} f(P_0) = 0 &= {P_e}^2 - \left(\frac{q_1^*(t)}{C_w}\right)^{\frac{1}{n}} - P_0(t)\sqrt{{P_e}^2 - \left(\frac{q_1^*(t)}{C_w}\right)^{\frac{1}{n}}} - a\left(\frac{q_1^*(t)}{C_v}\right)^2 \\ &= \sqrt{{P_e}^2 - \left(\frac{q_1^*(t)}{C_w}\right)^{\frac{1}{n}}} - P_0(t) - \frac{a\left(\frac{q_1^*(t)}{C_v}\right)^2}{\sqrt{{P_e}^2 - \left(\frac{q_1^*(t)}{C_w}\right)^{\frac{1}{n}}}}, \end{aligned} \tag{3.7}$$

where the flux value of flow $q_1^*(t)$ is obtained from (3.5) and is used in the calculation instead of the nodal flow $q_1(t)$ as recommended by Mennemann et al. (2018) for improved numerical stability of the model. Equation (3.7) is solved recursively for the boundary pressure $P_0(t)$.

It can be shown that equation $f(P_0)$ is a monotonically decreasing function by calculating $\frac{\partial f}{\partial P_0}$. Additionally it can be shown that (3.7) is positive for P_0 given by,

$$P_0 = P_1 - \frac{c}{A}q_1,$$

and that (3.7) is negative for P_0 given by,

$$P_0 = P_1 - \frac{c}{A}q_1 + c_w\frac{c}{A}{P_e}^{2n_w}.$$

These two opposite signed solutions combined with the monotonic nature of the function form numerically convergent initial values for a recursive numerical solver such as the modified Secant Method given by Ezquerro et al. (2024),

$$P_{0,n+1} = P_{0,n} - f(P_{0,n})\left(\frac{\theta P_{0,n} + (1-\theta)P_{0,n-1} - P_{0,n}}{f(\theta P_{0,n} + (1-\theta)P_{0,n-1}) - f(P_{0,n})}\right), \tag{3.8}$$

where an optimal value of $\theta = 0.9$ is chosen as found in Ezquerro et al. (2024).

3.2.2.2 Pipelines Connected to a Junction

The inlet boundary condition for pipelines connected to a junction shall be set as the pipe inlet flow rate $q_0(t)$. This flow will be calculated by making use of the conservation of mass at the junction. The outlet boundary condition shall be set as the pipeline outlet pressure which is determined by

downstream pipelines. The boundary conditions are therefore defined as,

$$\mathbf{B_L U}(0,t) = g_L(t) = q_0(t), \tag{3.9}$$

$$\mathbf{B_R U}(0,t) = g_R(t) = P_L(t). \tag{3.10}$$

Applying the CCM method to these boundary conditions results in,

$$\mathbf{F}^*(0,t) = \begin{bmatrix} q_1^*(t) \\ P_1^*(t) \end{bmatrix} = \begin{bmatrix} q_0 \\ P_1 + \frac{c}{A}(q_0 - q_1) \end{bmatrix}, \tag{3.11}$$

$$\mathbf{F}^*(L,t) = \begin{bmatrix} q_J^*(t) \\ P_J^*(t) \end{bmatrix} = \begin{bmatrix} q_J + \frac{A}{c}(P_J - P_L) \\ P_L \end{bmatrix}. \tag{3.12}$$

3.2.2.3 Pipelines Connecting Consumers to a Header

The inlet boundary condition for pipelines connecting a header to the consumer supply pipeline shall be set as the inlet flow. This flow will be calculated by making use of the conservation of mass at the header. The outlet boundary condition for this pipeline is the demand flow from the consumer. Therefore, the boundary conditions are given by,

$$\mathbf{B_L U}(0,t) = g_L(t) = q_0(t), \tag{3.13}$$

$$\mathbf{B_R U}(0,t) = g_R(t) = q_L(t). \tag{3.14}$$

Applying the CCM method to these boundary conditions results in,

$$\mathbf{F}^*(0,t) = \begin{bmatrix} q_1^*(t) \\ P_1^*(t) \end{bmatrix} = \begin{bmatrix} q_0 \\ P_1 + \frac{c}{A}(q_0 - q_1) \end{bmatrix}, \tag{3.15}$$

$$\mathbf{F}^*(L,t) = \begin{bmatrix} q_J^*(t) \\ P_J^*(t) \end{bmatrix} = \begin{bmatrix} q_L \\ P_J + \frac{c}{A}(q_J - q_L) \end{bmatrix}. \tag{3.16}$$

3.2.3 Natural Gas Production Network Block Diagram Representation

The boundary conditions defined in the previous sections are used to define an overall system model which is represented in block diagram form in Figure 3.2 to Figure 3.5. The block diagram representation of the natural gas network allows for modularity and ease of adaptation of the model to network changes as new component blocks can be added to the network when new wells are drilled and component blocks can be removed from the block diagram model when wells and pipelines are decommissioned.

The blocks named Choke & Well in Figure 3.2, Figure 3.3 and Figure 3.4 make use of Equation (3.7) to calculate the inlet boundary pressure for each pipe block. Three different types of pipeline blocks

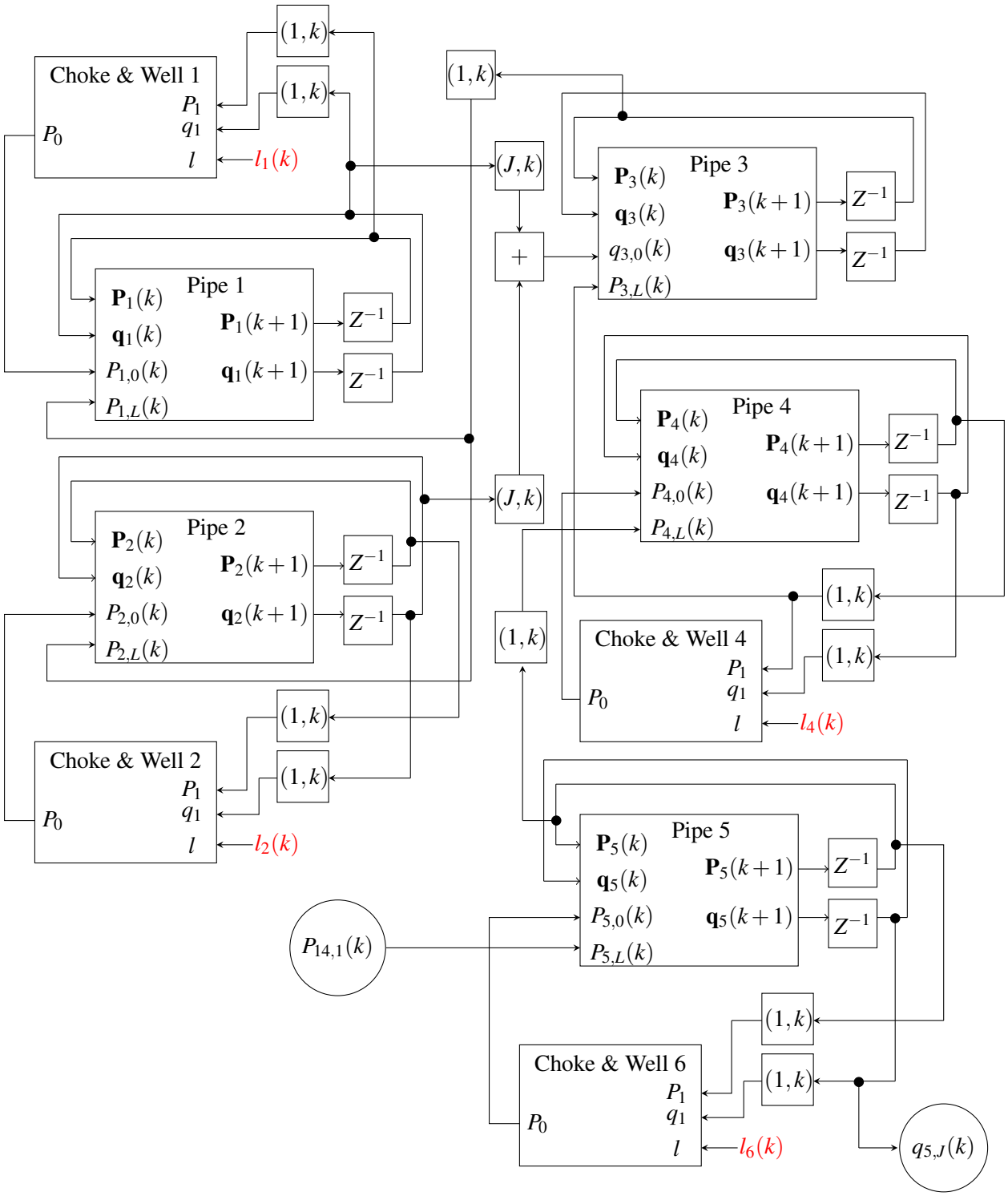

Figure 3.2. Natural Gas Production Network Simulation Block Diagram 1 of 4.

are used which differ in terms of their boundary conditions. These are defined in Section 3.2.2 as summarized below.

- Pipeline blocks with pipe inlet pressure $P_{i,0}(t)$ as the inlet boundary condition and pipe outlet pressure $P_{i,L}(t)$ as the pipe outlet boundary condition
- Pipeline blocks with pipe inlet flow rate $q_{i,0}(t)$ as the inlet boundary condition and pipe outlet pressure $P_{i,L}(t)$ as the pipe outlet boundary condition

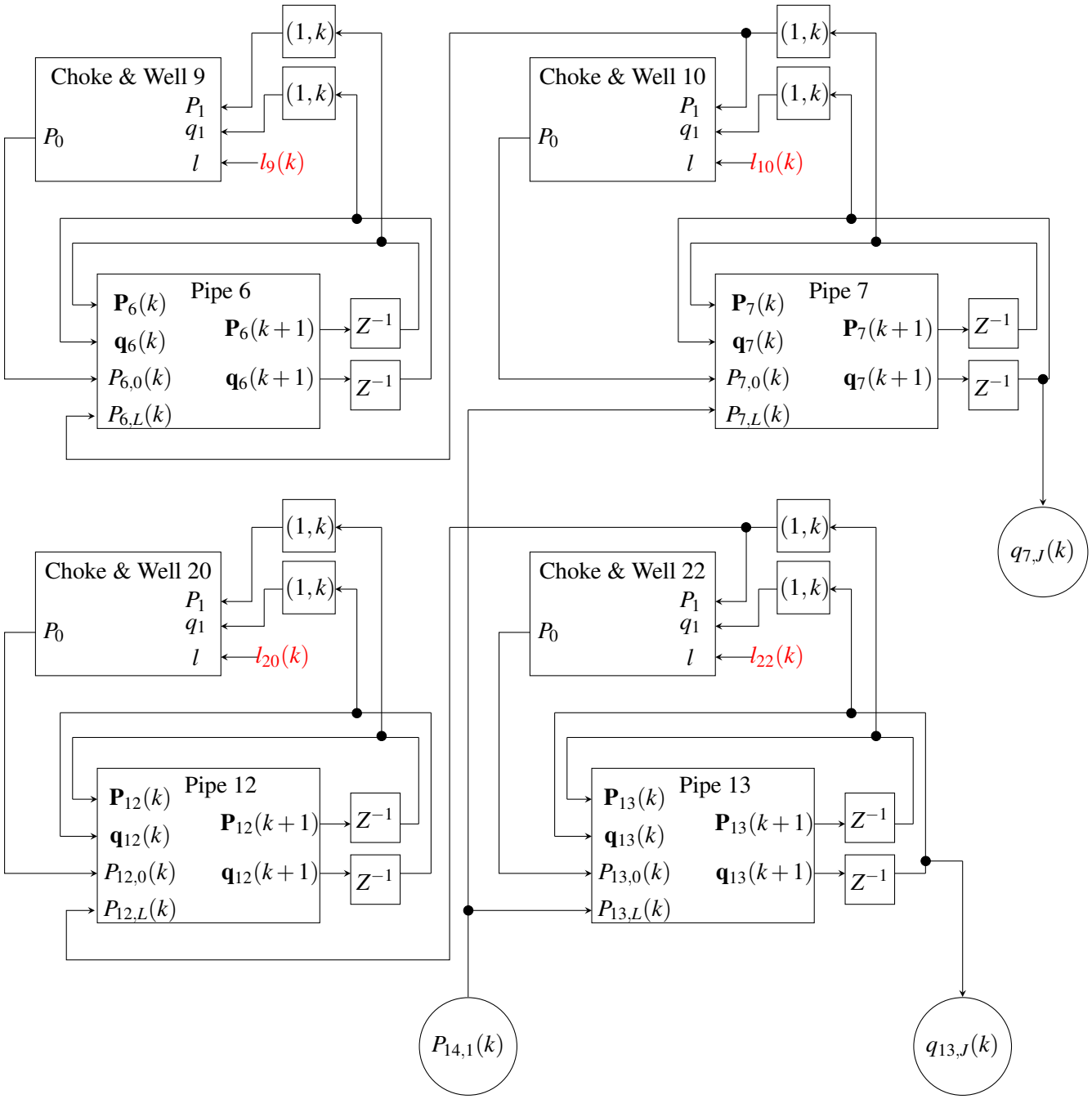

Figure 3.3. Natural Gas Production Network Simulation Block Diagram 2 of 4.

- Pipeline blocks with pipe inlet flow rate $q_{i,0}(t)$ as the inlet boundary condition and pipe outlet flow rate $q_{i,L}(t)$ as the pipe outlet boundary condition

Each pipe block calculates the pressure $\mathbf{P}_i(k+1)$ and flow rates $\mathbf{q}_i(k+1)$ using (2.28), (2.29), (2.64) and (2.65) in combination with the 4th order Runga-Kutta method for time discretization. It should be

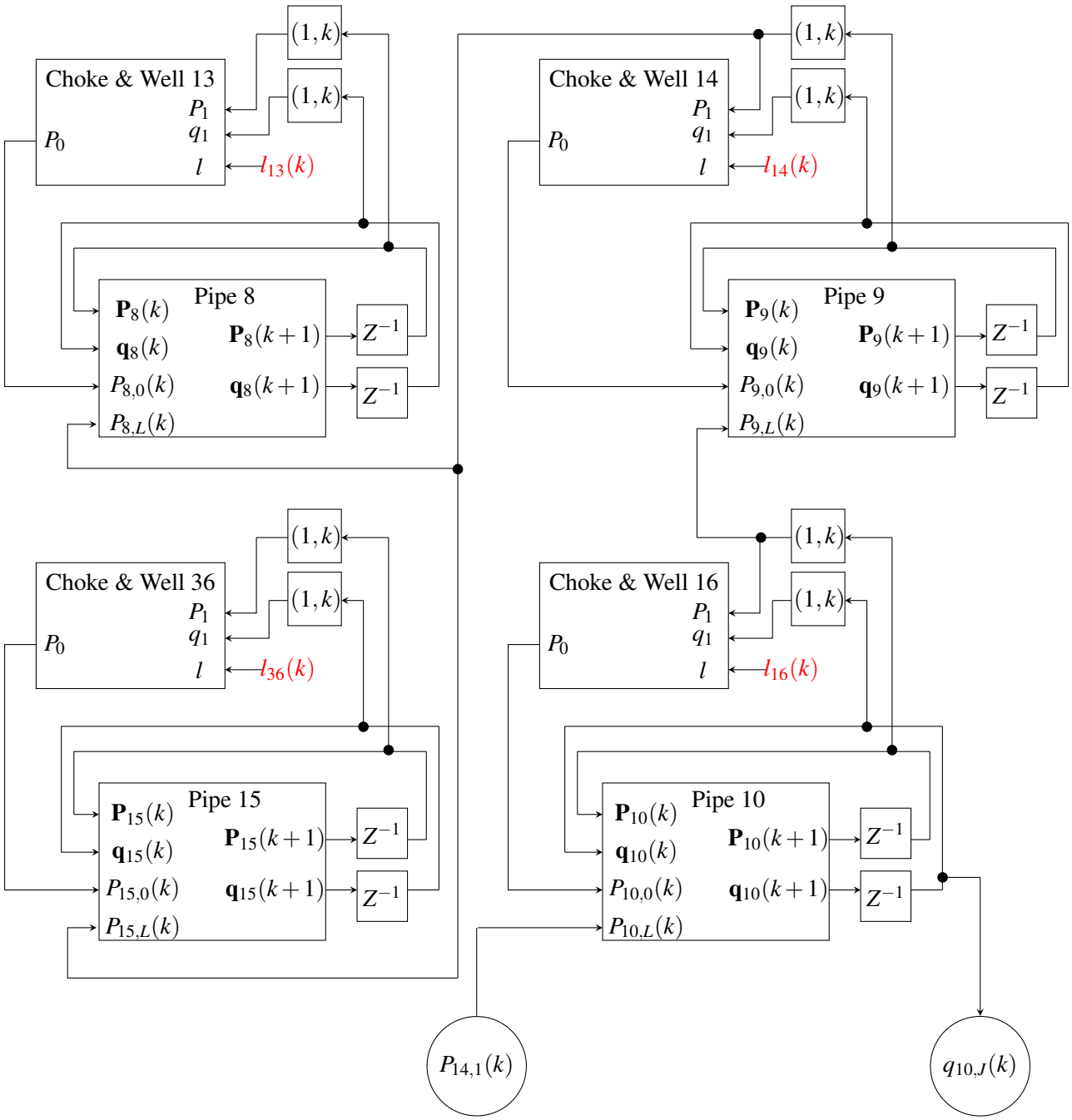

Figure 3.4. Natural Gas Production Network Simulation Block Diagram 3 of 4.

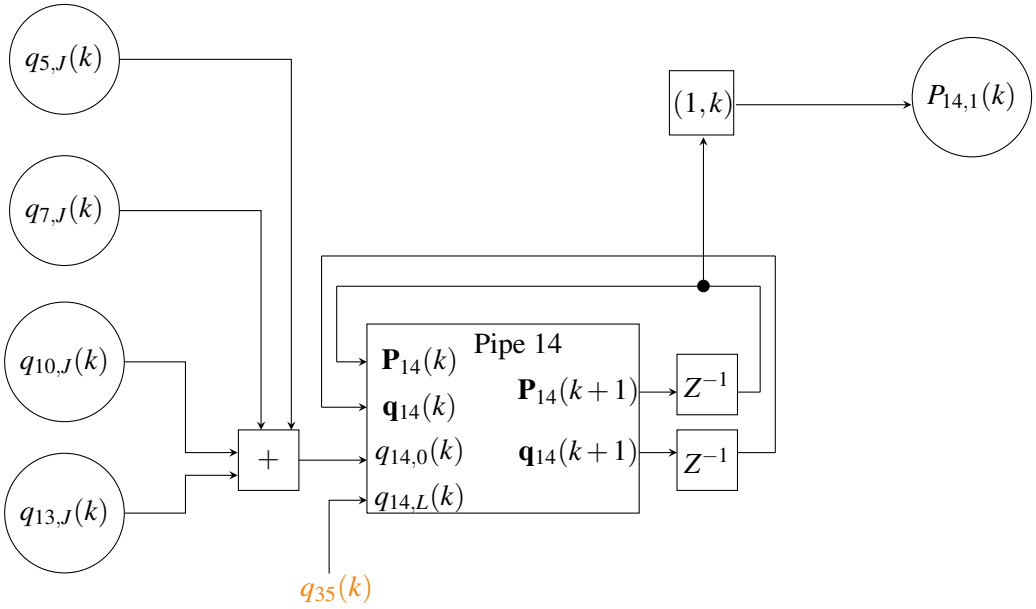

Figure 3.5. Natural Gas Production Network Simulation Block Diagram 4 of 4.

noted that operator Z^{-1} in the function block diagrams is a delay operator. The output of this operator is the block input value at the previous time instant i.e. $Z^{-1}(\mathbf{x_n}) = \mathbf{x_{n-1}}$.

3.3 MODEL PARAMETER ESTIMATION

The unknown model parameters in the natural gas production network were estimated from steady-state plant operating data. Due to the non-linear nature of these models, operating data that represents typical operating conditions have to be used in order to obtain a model that accurately captures the system response around the typical operating conditions. Models that contain unknown parameters for which parameter estimation is required are wellhead deliverability models and choke valve models.

3.3.1 Well Deliverability Model Parameter Estimation

The unknown parameters in the well deliverability model are obtained by making use of a mean square error estimation method given by,

$$\begin{bmatrix} C_w \\ n \end{bmatrix} = \arg\min_{C_w,n} \frac{1}{M} \sum_{m=0}^{M-1} (q - \hat{q})^2, \tag{3.17}$$

where $\hat{q}$ is given by (2.74), q is the measured gas flow rate from the well and M is the total number of measurements. It should be noted that in (2.74) the reservoir pressure P_e is known constant value.

3.3.2 Choke Valve Model Parameter Estimation

The unknown parameters in the choke valve models are also calculated by making use of a mean square error estimation method. The estimator used for each well choke valve is given by,

$$\begin{bmatrix} k_1 \\ k_2 \\ k_3 \\ k_4 \end{bmatrix} = \arg \min_{k_1,k_2,k_3,k_4} \frac{1}{M} \sum_{m=0}^{M-1} (q - \hat{q})^2. \tag{3.18}$$

where $\hat{q}$ is given by (2.75), and q is the measured gas flow rate through the choke valve.

3.4 SPECTRAL AND TIME DISCRETIZATION PARAMETER SETTINGS

Important parameters in the individual pipeline models are the number of spectral elements (M) and spectral polynomial order (N) for each pipeline. These values determine the spatial discretization length for each pipeline. A constraint is placed on the time discretization step size and spatial discretization length or number of nodes (J) based on the Courant-Friedrichs-Lewy (CFL) condition (Mennemann et al., 2018).

The system under consideration has different length pipelines. The shortest pipe element (pipeline #7 in Table 3.1) was used to determine the time discretization step. For this element the time discretization was chosen to be 0.5 s which resulted in a stable model for $N = 2$ and $M = 1$. For all other pipelines the values of N and M were estimated by increasing them until oscillation errors occurred at a fixed time step size of 0.5 s. The values of N and M obtained using this method are shown in Table 3.1.

3.5 CHAPTER CONCLUSION

The natural gas production network under consideration was fully described in this Chapter and presented in process flow diagram (PFD) form in Figure 3.1. The overall production network model was also developed and presented in block diagram form in Figure 3.2 to Figure 3.5. The production network PFD was converted into the system block diagram model by making use of the CCM method and suitable boundary conditions. The developed block diagram method will be used to perform dynamic simulations of the gas production network in Chapter 4. The block diagram form allows for a versatile modelling approach as it allows for ease of changing the model to cater for network changes. A method for estimating the unknown model parameters from plant data was also presented in this Chapter. The Chapter also presented the method used to obtain the SEM time and spacial descritization parameters. These parameters are the time discretization step size ΔT, number of spectral elements in each pipe (M) and number of nodes in each spectral element (N).

Table 3.1. Spatial Discretization Settings.

Pipeline #	N	M	L (m)
1	2	3	4480
2	2	2	2260
3	2	2	2960
4	2	2	4430
5	2	3	5200
6	3	3	4720
7	2	1	1400
8	3	4	5970
9	2	2	3900
10	2	4	3700
12	2	4	4300
13	3	4	9000
14	6	11	44800
15	2	4	3520

CHAPTER 4 MODEL VALIDATION AND PARAMETER ESTIMATION RESULTS

The aim of this Chapter is to validate the natural gas network block diagram model presented in Chapter 3 against data collected from an industrial natural gas production network. Section 4.1 describes the industrial data collected in order to perform model validation. This data was also used to estimate te values of unknown model parameters. The results of the model parameter estimation is presented in Section 4.2. The collected plant data was also used to correct the natural gas network model against errors in the calculated pipe friction factors. The friction factor correction method and resulting correction factors are presented in Section 4.3. Section 4.4 presents the model prediction results and a comparison of the model predictions and collected plant data based on a normalized root mean square (NRMS) error and, Pearson correlation coefficient matric.

4.1 INDUSTRIAL DATA

Plant data was collected for the industrial gas supply and distribution system shown in Figure 3.1 in order to develop and validate the model developed for the system. The collected modelling and validation datasets includes the consumer demand flow rate (q_{35}), consumer battery limit pressure (P_{35}), gas network header pressure (P_8), well tubing head pressures, choke valve outlet pressures, flow rates from each well and well choke valve command signals. The collected data was seperated into a training or identification set and a validation set as advised by Pillonetto et al. (2022). The training dataset is steady-state discontinuous data that was manually selected over a period of 8 months in order to develop the steady-state choke valve and steady-state well deliverability models. Periods where the well choke valves were being actuated or manipulated where selected from the 8 month period in order to ensure that accurate well and valve steady state models. The choke valve commands used to develop the steady state models are shown in Figure 4.1. Figure 4.1shows that the modelling period

contains sufficient MV movements to obtain an accurate well and choke valve model. However it can be seen that there MV variation data for choke valve 36 (l_{36}) and choke valve 1 (l_1) do not have sufficient movements for development of accurate models. Therefore, the overall system model will have reduced prediction accuracy for cases where these MVs are manipulated.

The validation dataset is dynamic data that was collected over a continuous period of 120 hours and was chosen to be separate from the training dataset periods. The continuous validation data was sampled at a rate of 5s for all measurements. The sampling period was chosen to coincide with the plant historian sampling frequency. The chosen sampling rate is sufficient to capture the dynamics of the process with no loss of information as the long pipelines result in a long system time constant (τ) of 1140 seconds. Goodwin and Payne (1977) recommend a sampling period of at most $5 \times \tau$ in order to ensure no loss of information. It should be noted that due to the long system time constant no measurement data

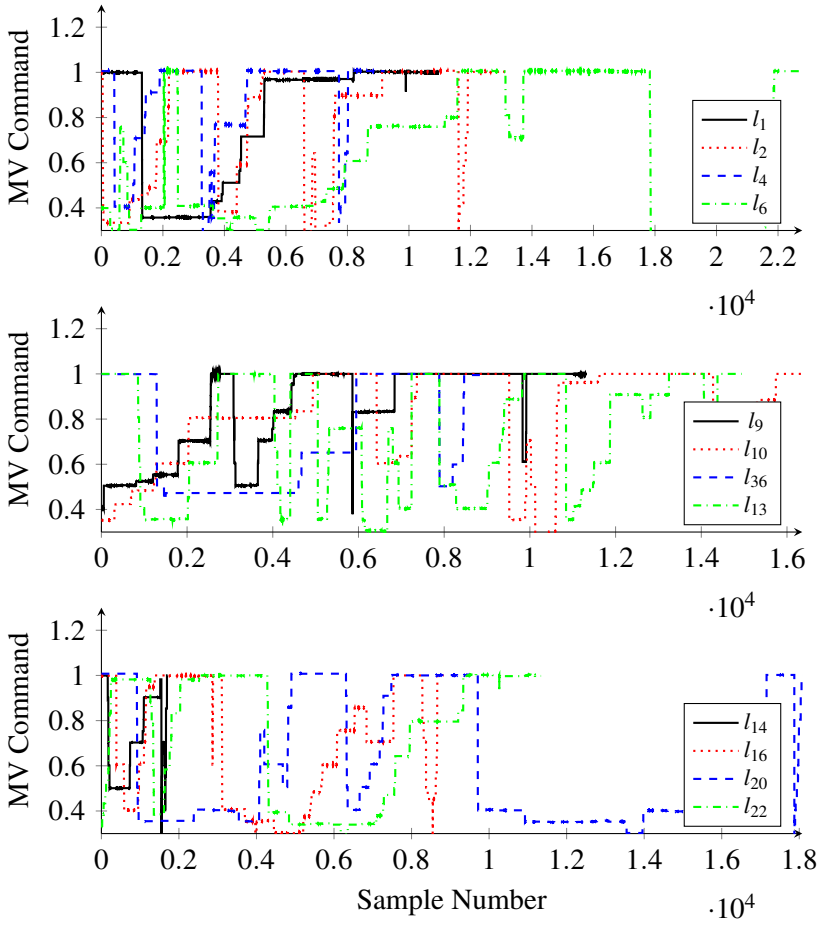

Figure 4.1. Well choke valve command measurements (normalized) over the model development period.

Table 4.1. Choke Valve and Well Deliverability Model Parameter Estimation Results.

Well #	C_w	n_w	k_1	k_2	k_3
1	1.654e-07	0.5695	0.008964	-0.005965	0.001366
2	1.167e-12	0.9626	-0.001439	0.002354	-0.0002721
4	1.133e-08	0.6676	-0.005364	0.008313	-0.002024
6	1.257e-16	1.266	0.004831	-0.0001033	0.0001665
9	2.571e-18	1.362	0.004256	-0.003166	0.0008038
10	6.526e-16	1.197	-0.001037	0.002208	-0.0001613
13	1.278e-20	1.609	0.006273	-0.0005336	0.0001143
36	3.398e-06	0.5067	-0.004633	0.007856	-0.00212
14	1.2e-16	1.239	0.001992	-0.0001154	9.776e-05
16	2.951e-16	1.251	0.003292	1.398e-05	0.0002872
20	3.293e-20	1.529	0.01014	-0.00411	0.0007463
22	4.238e-23	1.736	0.009269	-0.002869	0.0005286

filtering is required for the model validation data as all high frequency noise will be filtered by the system dynamics.

The system gas flow data over the validation period is shown in Figure 4.2. From Figure 4.2 it can be seen that the 120 hour period contains 5 periods of consumer flow or DV disturbances with different time durations and amplitudes therefore allowing for validation of the model over multiple transient time periods. The multiple transient conditions over the validation period increases the confidence of the model performance for periods outside the chosen validation period.

4.2 MODEL PARAMETER ESTIMATION RESULTS

The training dataset was used to develop the steady-state choke valve and steady-state well deliverability models based on (2.74) and (2.75). The result of the mean square error parameter estimations is shown in Table 4.1.

4.3 PIPELINE FRICTION FACTOR CORRECTION

Two error sources which can significantly affect the performance of the model are the friction factor calculated for each pipeline by (2.71) and the pipeline line lengths. A friction factor correction term $K_{g,i}$ was used to correct for these errors resulting in the friction factor used for pipeline i being given

Table 4.2. Friction Factor Correction Factors.

Pipeline #	K_g	Pipeline #	K_g
1	1	2	1
3	1	4	1.052
5	1.085	6	1.329
7	1.474	8	0.9122
15	1.026	9	1.246
10	1.001	12	2.24
13	1.196	14	0.9635

by,

$$\hat{f}_i = f_i K_{g,i},$$

where f_i is the pipeline friction factor calculated from (2.71). The friction factor correction factors $K_{g,i}$ were calculated by choosing a steady state operating point from the modelling dataset and using the steady state form of (2.6). The resulting friction correlation factor for pipeline i is given by,

$$K_{g,i} = \frac{A_i^2 D_i (P_L^2 - P_0^2)}{\bar{c}^2 q_i^2 L_i f_i}, \tag{4.1}$$

where P_L is the pipe outlet pressure, P_0 is the pipe inlet pressure, $\bar{c}$ is the average sound speed in pipeline i and, L_i is the length of pipeline i. The value of $K_{g,i}$ will be close to 1 if the friction factor calculated from (2.71) is accurate. The calculated friction factor correction factors are shown in Table 4.2.

4.4 MODEL VALIDATION RESULTS

The developed pipeline model as shown in model block diagrams 3.2, 3.3, 3.4 and 3.5 was used to predict the values of all CVs over the validation period as a pure simulation, i.e., no state or parameter updates were performed over the entire simulation period and only initial model state values were calculated from the validation data at the initial time $t = 0$. The normalized DV data (q_{35}) used in the model validation is shown in Figure 4.2. The choke valve commands over the validation period are shown in Figure 4.3 and relate to the MVs in Figure 3.1. Figure 4.2 and Figure 4.3 show that the validation period includes sufficient DV and MV variations to allow for the evaluation of the model prediction performance against DV and MV changes.

The model prediction results over the validation data period for the CVs are shown in Figure 4.4 to Figure 4.12. Variables shown in the figures relate to the CVs shown in Figure 3.1.

Figure 4.4 shows that the model is able to accurately predict the header pressure and consumer battery limit pressure in the presence of MV and DV changes. The simulation results in Figure 4.5 to Figure 4.8 show that the model can accurately predict the gas supply pressures from each well. The simulation results in Figure 4.9 to 4.12 also show that the developed model can accurately predict the gas flow rates from the wells. Figure 4.2 demonstrates the ability of the model to accurately capture the system dynamics as a dynamic lag can be observed between q_{34} and the consumer demand (q_{35}).

Table 4.3 evaluates the accuracy of the developed models according to the Pearson correlation coefficients ($\rho(y,\hat{y})$) between the plant measurements (y) and model predictions ($\hat{y}$), as well as the normalized root mean square errors for all CVs. The Pearson correlation coefficients for all CVs are greater than 0.94 which indicates the model is able to accurately capture the directionality of all CV movements. Table 4.3 shows that the pressure prediction NRMSE is less than 4.35% while the flow rate prediction NRMSE is less than 5.08%. The low NRMSE values show that the model has good CV prediction performance.

The pressure prediction results in Figure 4.4 to 4.8 show a prediction error at time $t = 36$ hours. This corresponds to a model response to a large change in consumer demand. The main source of these errors is due to uncertainties in the choke valve models caused by the scarcity of step test data required to develop accurate models. Figure 4.11 also shows a prediction error in the flow rate from well 36 at

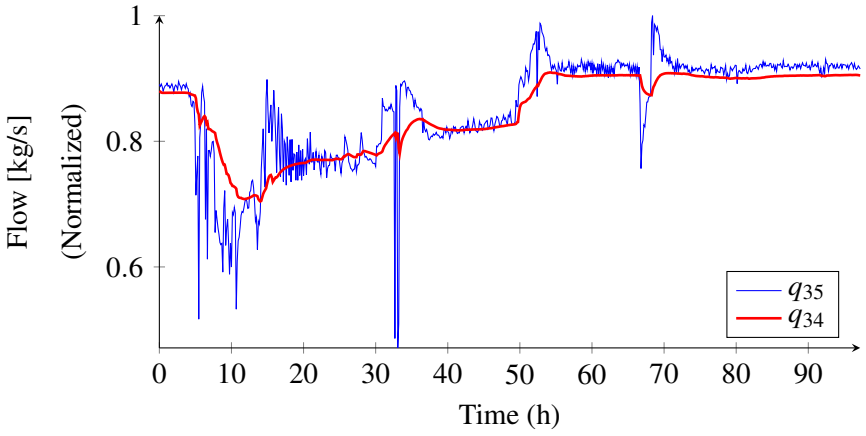

Figure 4.2. Consumer demand measurements over model validation period.

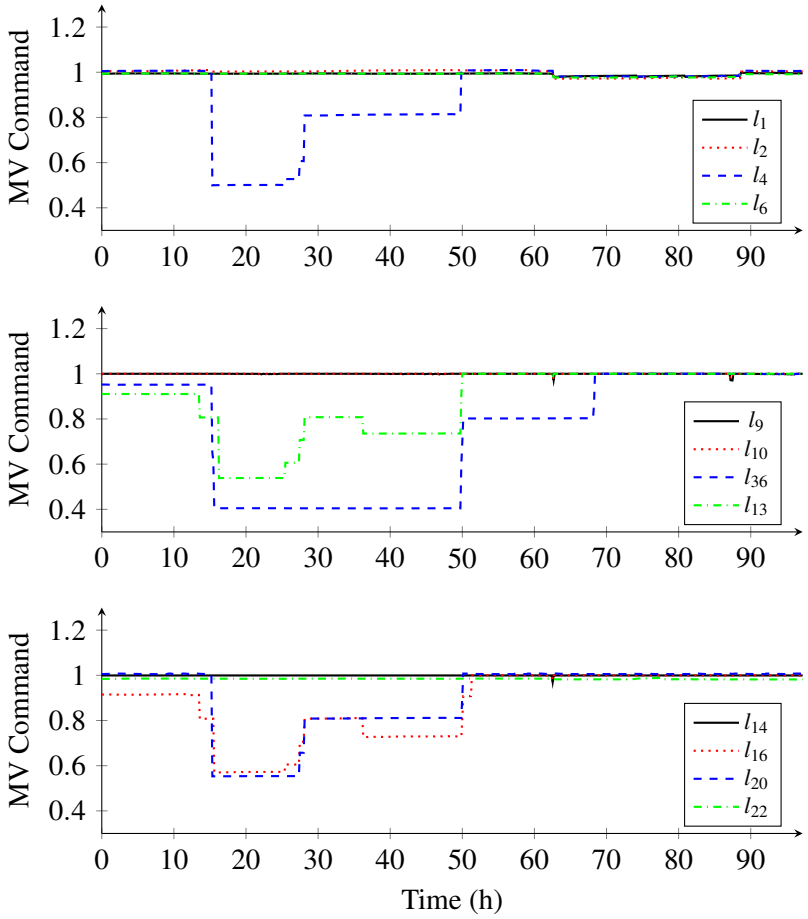

Figure 4.3. Well choke valve command measurements (normalized) over the model validation period.

time $t = 38$ hours. This also corresponds to a prediction error in the predicted pressure from well 36 as shown in Figure 4.7. The observed prediction errors on well 36 are due to the low amount of MV movements in the modelling data for choke valve 36 as seen in Figure 4.3. The NRMSE and Pearson correlation coefficient in Table 4.3 also show that the pressure and flow prediction for well 36 has the lowest Pearson correlation coefficient and highest NRMSE. The model for well 36 can be improved by performing step tests on the well in order to generate high quality modelling data with sufficient MV variations for the well. The model prediction errors result in Model-plant mismatch. However this Model-Plant mismatch can be mitigated as measurement feedback will be able to correct for the error in model based control applications.

The low correlation coefficient and NRMSE of the model predictions show that the model can be used for model based control applications with feedback correction. The developed model can also be used to investigate different model based control strategies for natural gas production networks in order

Table 4.3. Model prediction performance according to Pearson correlation coefficient and NRMSE.

Parameter	$\rho(y,\hat{y})$	NRMSE
P_8	0.9927	0.0304
P_{35}	0.9935	0.0435
P_1	0.9818	0.0366
q_1	0.9910	0.0157
P_2	0.9912	0.0206
q_2	0.9928	0.0487
P_4	0.9920	0.0264
q_4	0.9896	0.0361
P_6	0.9924	0.0291
q_6	0.9909	0.0249
P_9	0.9923	0.0273
q_9	0.9741	0.0433
P_{10}	0.9925	0.0270
q_{10}	0.9921	0.0432
P_{13}	0.9491	0.0297
q_{13}	0.9425	0.0249
P_{36}	0.9714	0.0320
q_{36}	0.9988	0.0508
P_{14}	0.9618	0.0229
q_{14}	0.9522	0.0272
P_{16}	0.9817	0.0268
q_{16}	0.9890	0.0459
P_{20}	0.9915	0.0282
q_{20}	0.9915	0.0455
P_{22}	0.9917	0.0279
q_{22}	0.9910	0.0195

to determine the most optimal control system schemes in terms of network pressure stability while maintaining operating constraints at each well.

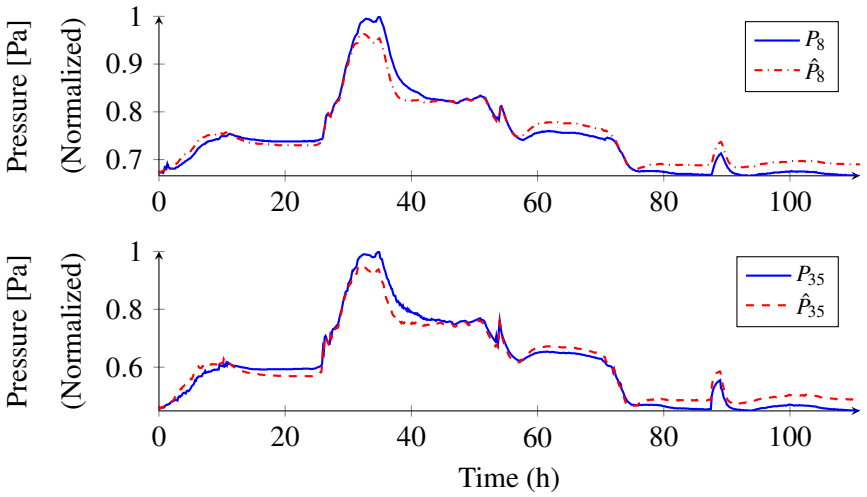

Figure 4.4. Model validation results for P_8 and P_{35}.

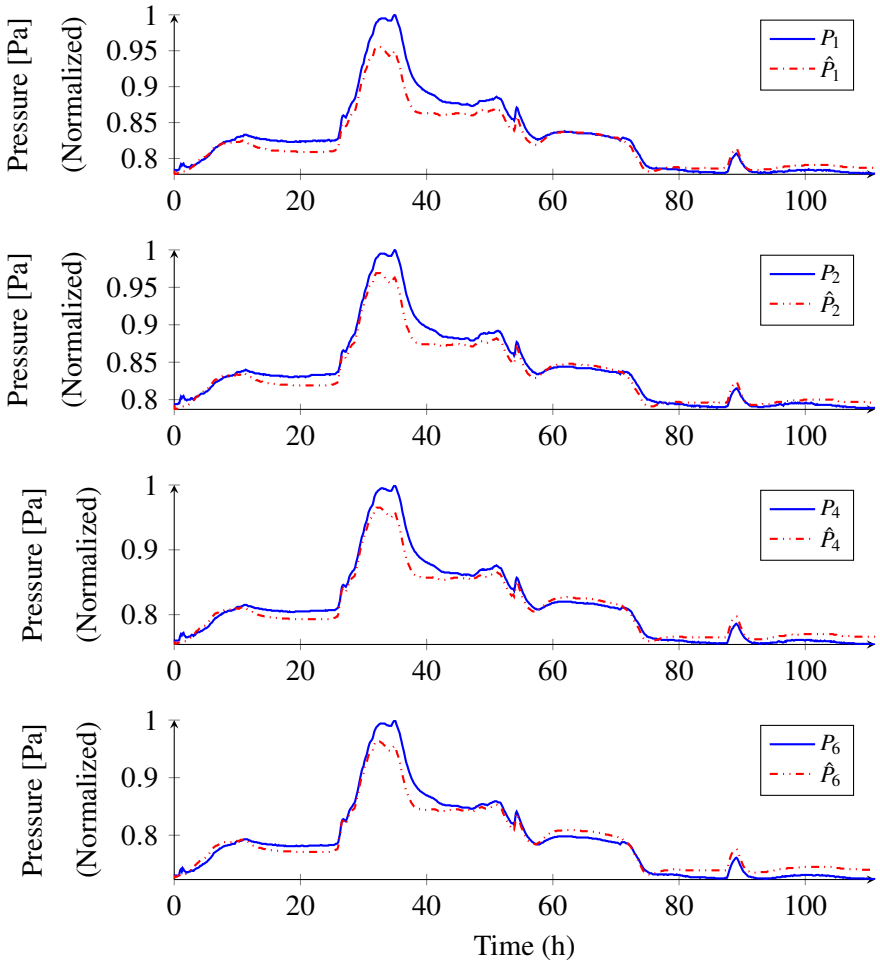

Figure 4.5. Model validation results for P_1, P_2, P_4 and P_6.

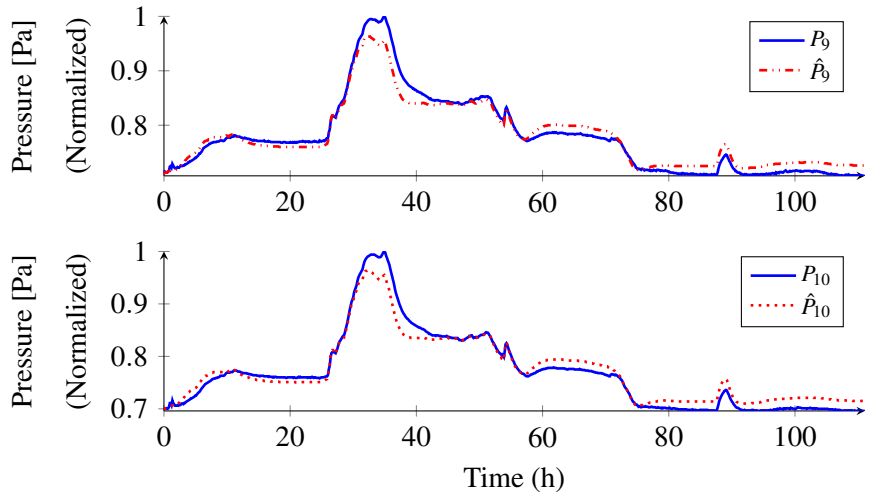

Figure 4.6. Model validation results P_9 and P_{10}.

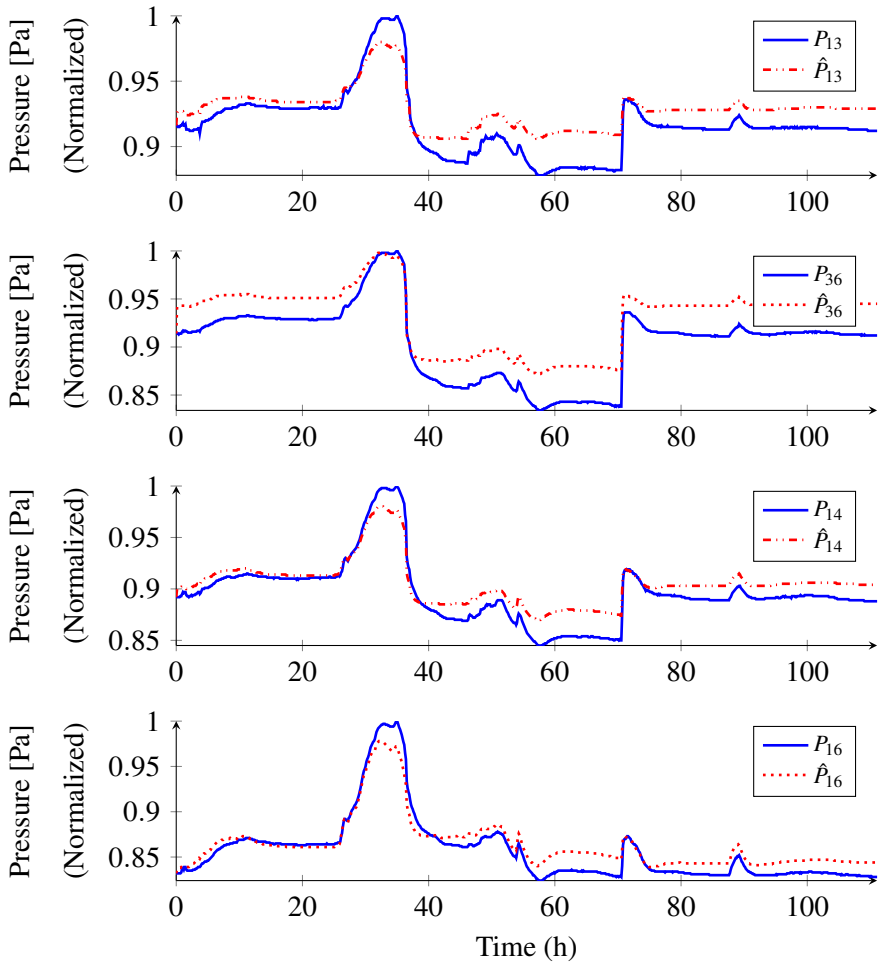

Figure 4.7. Model validation results P_{13}, P_{36}, P_{14} and P_{16}.

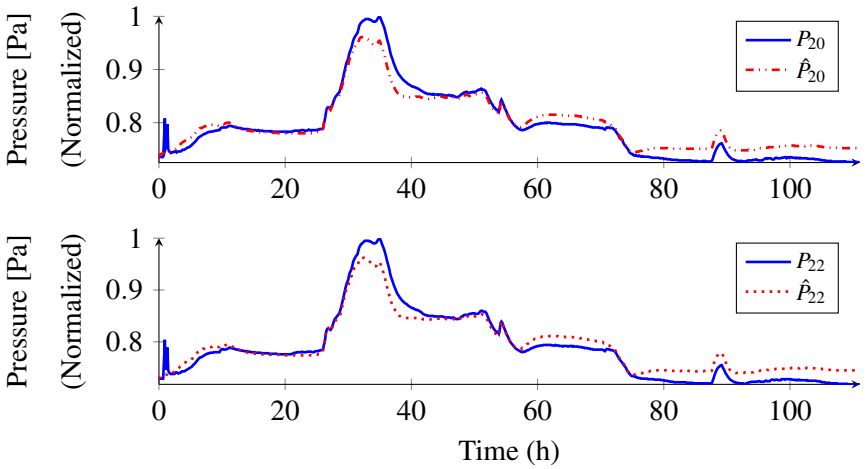

Figure 4.8. Model validation results for P_{20} and P_{22}.

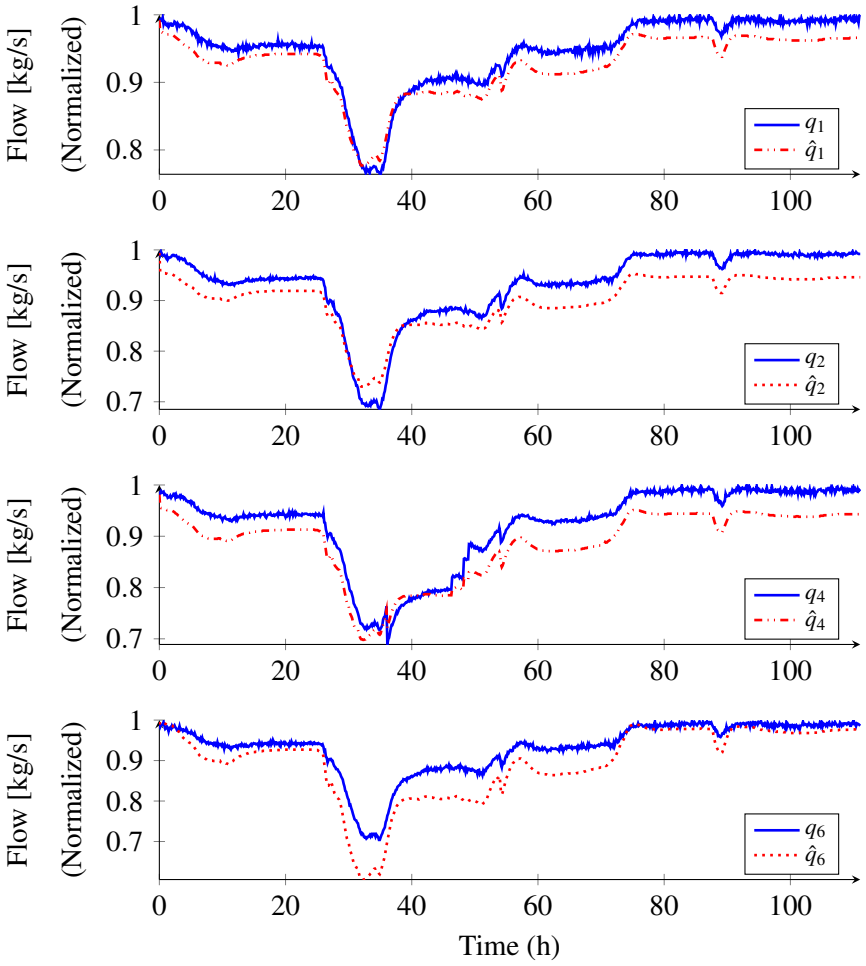

Figure 4.9. Model validation results for q_1, q_2, q_4 and q_6.

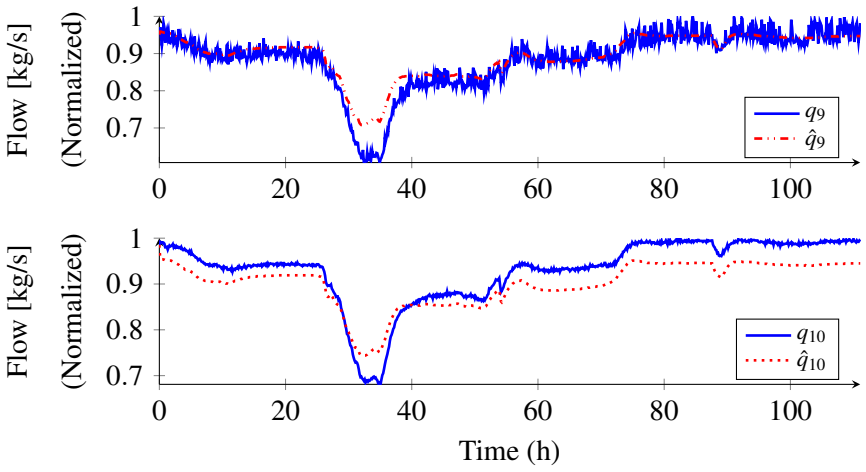

Figure 4.10. Model validation results for q_9 and q_{10}.

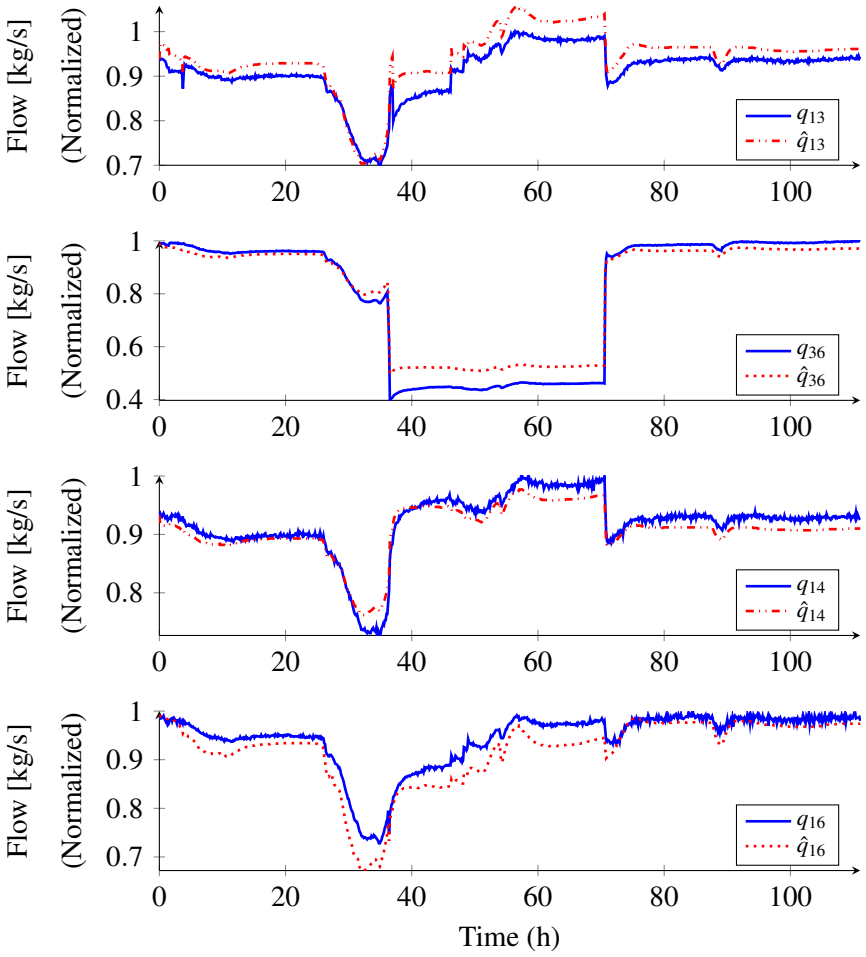

Figure 4.11. Model validation results for q_{13}, q_{14}, q_{36} and q_{16}.

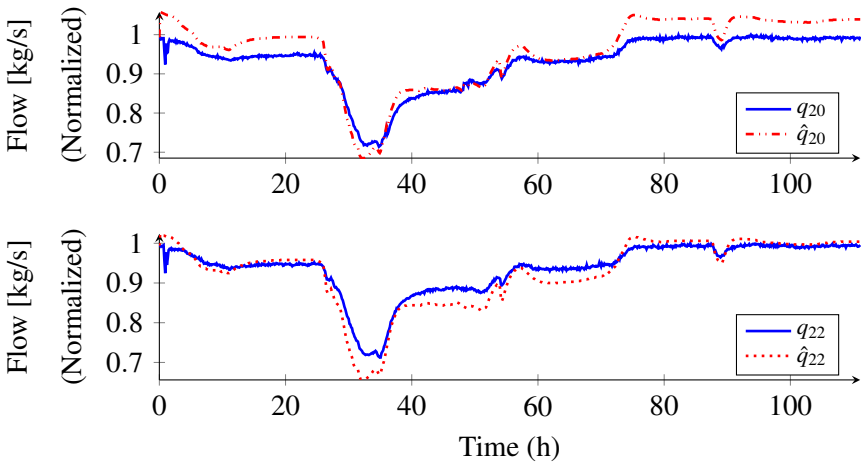

Figure 4.12. Model validation results for q_{20} and q_{22}.

4.5 CHAPTER CONCLUSION

The block diagram model developed in Chapter 3 was validated against industrial plant data from a natural gas production network. The collected plant data was used to calculate the values of unknown model parameters and correction factors for pipe friction factors. Manipulated and disturbance variable data was fed as inputs into the model to generate model predictions without the use of any feedback or model error corrections. The model was found to accurately predict the pressures and flow rates in the network. The model prediction results also show the suitability of using the model in model based control applications due to the high correlation coefficient between the model predictions and measured data.

CHAPTER 5 CONCLUSION

In this dissertation, SEM was used to develop a model of an industrial natural gas system made up of multiple gas wells and pipelines feeding one consumer. The gas production network model as shown in Figure 3.2 to Figure 3.5 was shown to produce accurate predictions of the flow rates from each well in the presence of choke valve and consumer demand changes. The gas production network model was shown to produce an accurate prediction of the consumer battery limit pressure and pressures at the well outlets based on a Pearson correlation coefficient of at most 0.94 and a normalized root mean square error of at most 5.08%. The good prediction performance of the gas production network model as shown from the high Pearson correlation coefficient shows that the model can be used for model based control applications.

In terms of future work, the developed model can be used to analyze the sensitivity of the model to model parameters such as compressibility, gas composition, temperature and viscosity in an attempt to simplify the model for reduced computational complexity. A model based controller can be implemented in order to demonstrate the benefit of implementing a model based controller on a natural gas well production network. The model can also be used to evaluate the effect of linearizing the model on the performance of a model based controller. Gas composition tracking can be added to model the scenario where gas from reservoirs with difference characteristics are mixed. Finally, the model can be improved to cater for changes in the gas temperature along the pipeline and junctions. This will increase the applicability of the model to more gas distribution systems such as systems with compressors and above ground piping.

REFERENCES

Achour, B. and Bedjaoui, A. (2012). Turbulent pipe-flow computation using the rough model method (rmm), *Journal of civil engineering and science* **1**: 36–41.

Bahadori, A. (2012). Estimation of flow coefficient for subsonic natural gas flow through orifice-type chokes using a simple method, *Journal of Natural Gas Science and Engineering* **9**: 39–44.

Bermúdez, A. and Shabani, M. (2019). Finite element solution of isothermal gas flow in a network, *Journal of Computational Physics* **396**: 616–652.

Bopbekov, D., Pourafshary, P. and Hazlett, R. (2022). Accuracy of droplet models for liquid loading prediction: Analysis of production well parameters, *Journal of Natural Gas Science and Engineering* **98**: 104391.

Burchell, J. J., Le Roux, J. D. and Craig, I. K. (2023). Nonlinear model predictive control for improved water recovery and throughput stability for tailings reprocessing, *Control Engineering Practice* **131**: 105385.

Canuto, C., Hussaini, M., Quarteroni, A. and Zang, T. (2006). *Spectral Methods: Fundamentals in Single Domains*, Springer, Verlag Berlin Heidelberg.

Canuto, C., Hussaini, M., Quarteroni, A. and Zang, T. (2007). *Spectral Methods: Evolution to Complex Geometries and Applications to Fluid Dynamics*, Springer, Verlag Berlin Heidelberg.

Chaczykowski, M. and Zarodkiewicz, P. (2017). Simulation of natural gas quality distribution for pipeline systems, *Energy* **134**: 681–698.

Climate Change Report for the year ended 30 June 2021 (2021). *Technical report*, Secunda, South Africa. https://www.sasol.com/sites/default/files/2022-05/Sasol%20Climate%20Change%20Report_2021_22Sep21.pdf, (accessed: 2023-08-30).

Darby, M. L. and Nikolaou, M. (2012). MPC: Current practice and challenges, *Control Engineering Practice* **20**(4): 328–342.

Dzedzemane, R., Wiid, A. J., le Roux, J. D. and Craig, I. K. (2024). Natural gas well production network state-space model development and validation for process control, *Industrial & Engineering Chemistry Research* **63**(3): 1461–1473.

Ekechukwu, G. K. and Orodu, O. D. (2019). Novel mathematical correlation for accurate prediction of gas compressibility factor, *Natural Gas Industry B* **6**(6): 629–638.

Ezquerro, J., Hernandez-Veron, M., Magrenan, A. and Moysi, A. (2024). A procedure to obtain quadratic convergence from the secant method, *Journal of Computational and Applied Mathematics* **448**: 115912.

Fang, J., Zeng, Q., Ai, X., Chen, Z. and Wen, J. (2018). Dynamic optimal energy flow in the integrated natural gas and electrical power systems, *IEEE Transactions on Sustainable Energy* **9**(1): 188–198.

Goodwin, G. C. and Payne, R. L. (1977). *Dynamic system identification : experiment design and data analysis.*, Communications and Control Engineering, Academic Press, New York, chapter 6.

Grace, A. and Frawley, P. (2011). Experimental parametric equation for the prediction of valve coefficient (cv) for choke valve trims, *International Journal of Pressure Vessels and Piping* **88**(2): 109–118.

Guedes, P. F., Lacerda, M. J. and Nepomuceno, E. (2024). State-feedback control design for polynomial discrete-time systems obtained via second-order runge-kutta discretization, *IFAC-PapersOnLine* **58**(5): 13–19.

Guo, B. and Ghalambor, A. (2012). *Natural Gas Engineering Handbook*, 2 edn, Gulf Publishing Company, Houston, Texas.

International Society of Automation (2007). Flow equations for sizing control valves, *Technical report*.

International Energy Agency (n.d.). https://www.iea.org/data-and-statistics/data-product/electricity-information. (accessed: 2023-08-30).

Kareem, L. A., Iwalewa, T. M. and Al-Marhoun, M. (2016). New explicit correlation for the compressibility factor of natural gas: linearized z-factor isotherms, *Journal of Petroleum Exploration and Production Technology* **6**(3): 481–492.

Kessal, M. (2000). Simplified numerical simulation of transients in gas networks, *Chemical Engineering Research and Design* **78**(6): 925–931.

Koo, B. (2022). Comparison of finite-volume method and method of characteristics for simulating transient flow in natural-gas pipeline, *Journal of Natural Gas Science and Engineering* **98**: 104374.

Loegering, M. J. and Milkov, A. V. (2017). Geochemistry of petroleum gases and liquids from the Inhassoro, Pande and Temane fields onshore Mozambique, *Geosciences* **7**(2): 33.

Mennemann, J.-F., Marko, L., Schmidt, J., Kemmetmüller, W. and Kugi, A. (2018). The spectral element method as an efficient tool for transient simulations of hydraulic systems, *Applied Mathematical Modelling* **54**: 627–647.

Muller, C. J., Craig, I. K. and Ricker, N. L. (2011). Modelling, validation, and control of an industrial fuel gas blending system, *Journal of Process Control* **21**(6): 852–860.

Nejatian, I., Kanani, M., Arabloo, M., Bahadori, A. and Zendehboudi, S. (2014). Prediction of natural gas flow through chokes using support vector machine algorithm, *Journal of Natural Gas Science and Engineering* **18**: 155–163.

Peng, D.-Y. and Robinson, D. B. (1976). A new two-constant equation of state, *Industrial & Engineering Chemistry Fundamentals* **15**(1): 59–64.

Pillonetto, G., Chen, T., Chiuso, A., De Nicolao, G. and Ljung, L. (2022). *Regularized system identification. Learning dynamic models from data*, Communications and Control Engineering, Springer, Cham, Switzerland, chapter 2.

Romeo, E., Royo, C. and Monzón, A. (2002). Improved explicit equations for estimation of the friction factor in rough and smooth pipes, *Chemical Engineering Journal* **86**(3): 369–374.

Smith, R. (1961). Unsteady-state gas flow into gas wells, *Journal of Petroleum Technology* **13**(11): 1151–1159.

Soave, G. (1972). Equilibrium constants from a modified redlich-kwong equation of state, *Chemical Engineering Science* **27**(6): 1197–1203.

Starling, K. and Savidge, J. (1994). *Compressibility Factors of Natural Gas and Other Related Hydrocarbon Gases*, Transmission Measurement Committee Report, 2 edn, AGA, American Gas Association, Arlington, Va.

Strambo, C., Burton, J. and Atteridge, A. (2019). The end of coal? Planning a "just transition" in South Africa, *Technical report*, Stockholm, Sweden. https://www.sei.org/publications/the-end-of-coal-planning-a-just-transition-in-south-africa/, (accessed: 2023-08-30).

Su, H., Zio, E., Zhang, Z.-J., Xiong, C.-Z., Dai, Q.-S., Wu, Q.-W. and Zhang, J.-J. (2022). Development of an integrated dynamic model for supply security and resilience analysis of natural gas pipeline network systems, *Petroleum Science* **19**(2): 761–773.

The role of gas as a transition fuel in South Africa's path to net-zero (2022). *Technical report*, Sandton, South Africa. https://www.nbi.org.za/climate-pathways-and-a-just-transition-for-south-africa/, (accssed: 2023-08-30).

Tordoir, P. (2022). Is natural gas the next coal? A framework for utilities and governments to think about the place of natural gas in the energy mix, *The Electricity Journal* **35**(2): 107077.

Trapp, C., Casella, F. and Colonna, P. (2014). Dynamic modeling and validation of a precombustion C02 capture plant for control design, *Industrial & Engineering Chemistry Research* **53**(33): 13098–13111.

Twyman, J. (2018). Transient flow analysis using the method of characteristics MOC with five-point interpolation scheme, *Obras y Proyectos* **24**: 62–70.

van de Haar, A., Trapp, C., Wellner, K., de Kler, R., Schmitz, G. and Colonna, P. (2017). Dynamics of postcombustion CO2 capture plants: Modeling, validation, and case study, *Industrial & Engineering Chemistry Research* **56**(7): 1810–1822.

Vatankhah, A. R. (2014). Comment on "gene expression programming analysis of implicit colebrook–white equation in turbulent flow friction factor calculation", *Journal of Petroleum Science and Engineering* **124**: 402–405.

Walters, M. S., Lin, Y.-J., Sachde, D. J., Edgar, T. F. and Rochelle, G. T. (2016). Control relevant model of amine scrubbing for CO2 capture from power plants, *Industrial & Engineering Chemistry Research* **55**(6): 1690–1700.

Wang, X. and Economides, M. (2009). *Advanced Natural Gas Engineering*, Gulf Publishing Company, Houston, Texas.

Wiid, A. J., Le Roux, J. D. and Craig, I. K. (2020). Modelling of methane-rich gas pipeline networks for simulation and control, *Journal of Process Control* **92**: 234–245.

Yang, X., Zhang, S. and Zhu, W. (2017). A new model for the accurate calculation of natural gas viscosity, *Natural Gas Industry B* **4**(2): 100–105.

Zeghadnia, L., Robert, J. L. and Achour, B. (2019). Explicit solutions for turbulent flow friction factor: A review, assessment and approaches classification, *Ain Shams Engineering Journal* **10**(1): 243–252.

Zienkiewicz, O. and Taylor, R. (2000). *The Finite Element Method Fifth Edition. Volume 3: Fluid Dynamics*, Butterworth-Heinemann, Linacre House, Jordan Hill, Oxford.

Zigrang, D. J. and Sylvester, N. D. (1982). Explicit approximations to the solution of colebrook's friction factor equation, *AIChE Journal* **28**(3): 514–515.